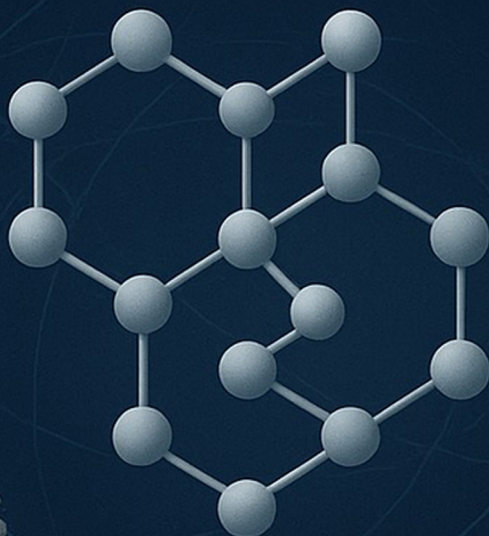


MULTIFUNCTIONAL MATERIALS THROUGH SURFACE ENGINEERING AND ALLOYING TECHNIQUES



Edited by
Assoc. Prof. Dr. Mehmet AKKAŞ



**MULTIFUNCTIONAL MATERIALS
THROUGH SURFACE ENGINEERING AND
ALLOYING TECHNIQUES**

Editor

Assoc. Prof. Dr. Mehmet AKKAŞ



Multifunctional Materials through Surface Engineering and Alloying Techniques

Editor: Assoc. Prof. Dr. Mehmet AKKAŞ

Editor in chief: Berkan Balpetek

Cover and Page Design: Duvar Design

Printing : June -2025

Publisher Certificate No: 49837

ISBN: 978-625-5885-55-5

© Duvar Yayınları

853 Sokak No:13 P.10 Kemeraltı-Konak/İzmir

Tel: 0 232 484 88 68

www.duvar yayinlari.com

duvarkitabevi@gmail.com

TABLE OF CONTENTS

Chapter 1.....5

COATING OF ARMOX 500 STEEL WITH TiC POWDERS BY THE THERMO-REACTIVE DIFFUSION METHOD

İhsan KIRIK

Chapter 2.....25

PRODUCTION and FRICTION PROPERTIES of Al, Mg and Ti ALLOY CARBIDE REINFORCED COMPOSITES USING POWDER METALLURGY-A REVIEW

İhsan KIRIK

Chapter 3.....43

SURFACE COATING TECHNIQUES

Adnan KESKİN, Musa KILIÇ

Chapter 4.....57

MORPHOLOGICAL AND TRIBOLOGICAL COMPARISON OF FE-BASED COATING AND Fe-WC COMPOSITE COATING IN LASER CLADDING METHOD

Fatih DEMİR, Mehmet EROĞLU, Necmettin IŞIK

Chapter 5.....57

DEVELOPMENT AND MICROSTRUCTURAL EVALUATION OF MECHANICALLY ALLOYED HIGH-ENTROPY ALLOYS SYNTHESIZED BY POWDER METALLURGY

Mehmet AKKAŞ

Chapter 1

COATING OF ARMOX 500 STEEL WITH TiC POWDERS BY THE THERMO-REACTIVE DIFFUSION METHOD

İhsan KIRIK¹

¹ Prof. Dr., Department of Machinery and Metal Technologies, Bingol University, Turkey,
ikirik@bingol.edu.tr, (ORCID: 0000-0002-8361-319X)

INTRODUCTION

Armor-grade steels are vital to the defense sector due to their ability to endure extreme impact forces. These steels are extensively utilized in applications demanding top-tier ballistic protection, including military aircraft, armored vehicles, battle tanks, and personal gear shielding against firearms and explosive devices. Among them, Armox 500-a type of ultra-high-strength steel-distinguishes itself through exceptional toughness and high hardness. However, its susceptibility to cracking under cyclic loading conditions can be reduced by reinforcing the surface with hard coatings. For instance, Youssef et al. explored the effects of niobium (Nb) micro-alloying and refined austenite grain structures on Armox 500T steel, utilizing a specific heat treatment cycle. Their results demonstrated that Nb addition significantly enhanced hardness and wear resistance. Similarly, Altuncu applied martensitic stainless steel powder coatings via laser cladding on armor steel surfaces [1-8]. The base material had an average hardness of approximately 400 ± 20 HV0.3, whereas the coated layer reached around 620 ± 50 HV0.3, owing to the presence of hard phases formed during the process. Surface coatings not only increase microhardness and wear resistance but also improve corrosion resistance and reduce the coefficient of friction. Techniques such as laser cladding, TIG welding, HVOF, PVD, and SHS are commonly used for this purpose. However, these methods often involve complex equipment setups, operational challenges, and high costs, which limit their widespread application. As a more accessible and environmentally friendly alternative, the thermo-reactive diffusion (TRD) method offers a simpler approach to enhancing surface properties. TRD processes create robust, wear- and corrosion-resistant coatings through chemical reactions between the steel surface and added elements like vanadium, chromium, niobium, or titanium [9-14]. These elements form hard carbides, nitrides, or carbonitrides by reacting with carbon and nitrogen from the steel and surrounding medium. However, TRD is typically applicable only to steels containing more than 3% combined carbon and nitrogen by weight. In prior research, Islak et al. applied boron-based coatings to engine valve surfaces using TRD, showing that increased temperature and time enhanced phase formation, despite a reduction in boron content. Substrate hardness was measured at 200 HV0.2, while plasma-nitrided layers and mixed nitride coatings reached up to 1655 HV0.2. Efe et al. formed a titanium boride coating on a Ti6Al4V alloy with a maximum thickness of 16 μm and hardness above 2000 HV. The layer growth exhibited a parabolic relationship with treatment time and temperature. Likewise, Topuz et al. successfully produced chromium carbide coatings on tool and nitriding steels without any signs of cracking or delamination at the interface [15-21]. Xiao et al. demonstrated that

vanadium carbide coatings on M35 high-speed steel reached a surface hardness of 2644 HV—over 250% higher than the base material—and yielded an 82.8% improvement in wear resistance. Günen et al. observed that increasing treatment duration and temperature boosted vanadium content and improved wear resistance in CrVC coatings on AISI D2 steel. Among transition metal compounds, titanium carbide (TiC) stands out for its excellent thermal stability, low density, high hardness, and superior wear and corrosion resistance, as well as its strong adhesion to iron substrates. Research shows that carbon diffusion promotes TiC phase formation, which can increase wear resistance by over 128%. Buytoz et al. produced TiC coatings on AISI 4140 steel using TRD and detected both TiC and α -Fe phases. Coating thickness ranged from 3.04 to 11.70 μm , with hardness values between 1089 and 2335 HV. Similarly, Kılıç reported a peak microhardness of 1301 HV after 3 hours of TiC treatment on AISI 4140 steel [22-27]. Despite rising interest in surface modification, studies focusing on TiC coatings for Armox 500 remain scarce. This study addresses that gap by investigating the enhancement of Armox 500 steel's surface properties via TRD-applied TiC coatings. The coatings were applied at three different temperatures (950°C, 1000°C, and 1050°C) and for three time intervals (1, 2, and 3 hours). Post-treatment analysis involved optical microscopy (OM), scanning electron microscopy (SEM), X-ray diffraction (XRD), and energy-dispersive spectroscopy (EDS). Microhardness tests were also conducted. The coating layers formed showed strong adhesion and uniform distribution across the substrate. Coating thickness increased with temperature and time, ranging from 2.591 μm (950°C, 1 hour) to 9.148 μm (1050°C, 3 hours). The highest recorded microhardness was 3036 HV0.5 at 1050°C after 3 hours. XRD confirmed the formation of TiC, TiO₂, and α -Fe phases. The substantial increase in surface hardness was attributed to the development of these hard carbides within the coating [28-30].

1. EXPERIMENTAL STUDIES

Armox 500 steel, cut into dimensions of 12×12×10 mm, was selected as the substrate material (see Table 1). After cutting, the substrate surfaces were polished sequentially with sandpapers of grit sizes ranging from 120 to 1200 mesh. Following polishing, the samples were cleaned in an alcohol bath to eliminate any dirt and contaminants. Titanium carbide (TiC) powder, with an average particle size of about 45 μm (shown in Figure 1), was used as the coating material. To obtain a uniform coating mixture, powders comprising 45 wt% FeTi, 45 wt% Al₂O₃, and 10 wt% NH₄Cl were blended using a mixing apparatus and then prepared for the coating application.

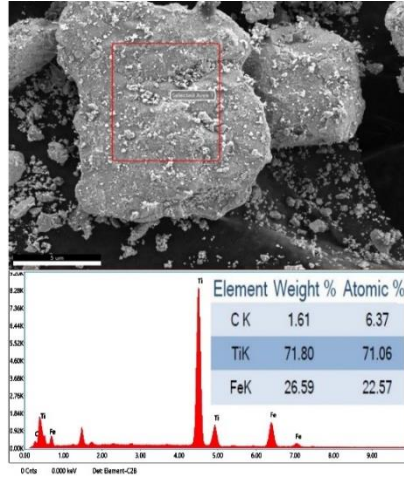


Figure 1. SEM and EDS analysis image of FeTi powder

Table 1. Chemical composition of ARMOX 500 armor steel

Chemical Content (%)									
Alloy	C	Si	Mn	P	S	Cr	Ni	Mo	B
Armox500	0,32	0,4	1,2	0,010	0,003	1,01	1,81	0,70	0,005

The samples, whose polishing process was completed, were buried in the mixture powder in the crucible, the mouth of the crucible was tightly closed and the surrounding area was plastered with heat-insulating mud.



Figure 2. Schematic view of the TRD coating process

The crucibles depicted in the schematic diagram (Figure 2) were placed in a high-temperature furnace and subjected to coating processes at 950 °C, 1000 °C, and 1050 °C for durations of 1, 2, and 3 hours, respectively. Each thermal cycle involved a three-step heating protocol: initially to 350 °C, then 700 °C, and finally to the designated process temperature. Upon completion of the heat treatment, the crucibles were water-quenched to room temperature. The coated samples were subsequently extracted and prepared for metallographic examination. Sample preparation began with mounting using a Metkon Ecompress 50 hot mounting press. Coarse grinding was performed using abrasive SiC papers ranging from 120 to 2500 grit until the base material was exposed. A Multipol Advanced automatic grinding and polishing system was employed, applying 1.5 bar of pressure during grinding and 0.6 bar during polishing. Fine polishing followed, using a DiMaxx Mono 9 μm diamond suspension with an Aka-Allegran disc, and final polishing was conducted with a Diadouble Mono 1 μm suspension for 420 seconds to enhance microstructural clarity. To reveal microstructural features, specimens were etched with 3% Nital solution. Microstructural characterization was carried out using an Eclipse MA 100 optical microscope and a JEOL JSM-5600 scanning electron microscope (SEM) coupled with energy-dispersive X-ray spectroscopy (EDS) for elemental analysis. Phase identification of hard carbide compounds within the coating layer was performed using X-ray diffraction (XRD) on a Bruker AXS D8 Advance diffractometer operated at 40 kV and 40 mA, scanning in the 2θ range of 20°–90°. Microhardness measurements were conducted using a Future Tech FM700 digital microhardness tester at three distinct regions: the substrate, the interface, and the coating layer.

2. EXPERIMENTAL RESULTS AND EVALUATION

2.1. Microstructure Analysis

Figure 3 displays optical micrographs of coatings produced via the thermal diffusion method at three distinct temperatures, all held for a constant duration of 2 hours. A strong metallurgical bond was achieved between the coating layer and the substrate across all samples. The interface appeared smooth, without cracks or porosity. At 950 °C, the coating exhibited a tooth-like, wavy morphology, whereas coatings formed at 1000 °C and 1050 °C were more uniform and smoother. Increasing the temperature resulted in a more consistent and regular interface between the coating and substrate surfaces. In the TRD process, the primary mechanism responsible for the robust adhesion at higher temperatures is believed to be the upward diffusion of free carbon atoms from the substrate, which subsequently react with titanium to create bonding phases. As illustrated

in Figure 3c, a notably high density of martensitic laths is visible within the substrate's microstructure. This is due to the use of a high-strength hardened steel substrate and the water quenching performed after heat treatment, which accelerated martensite formation.

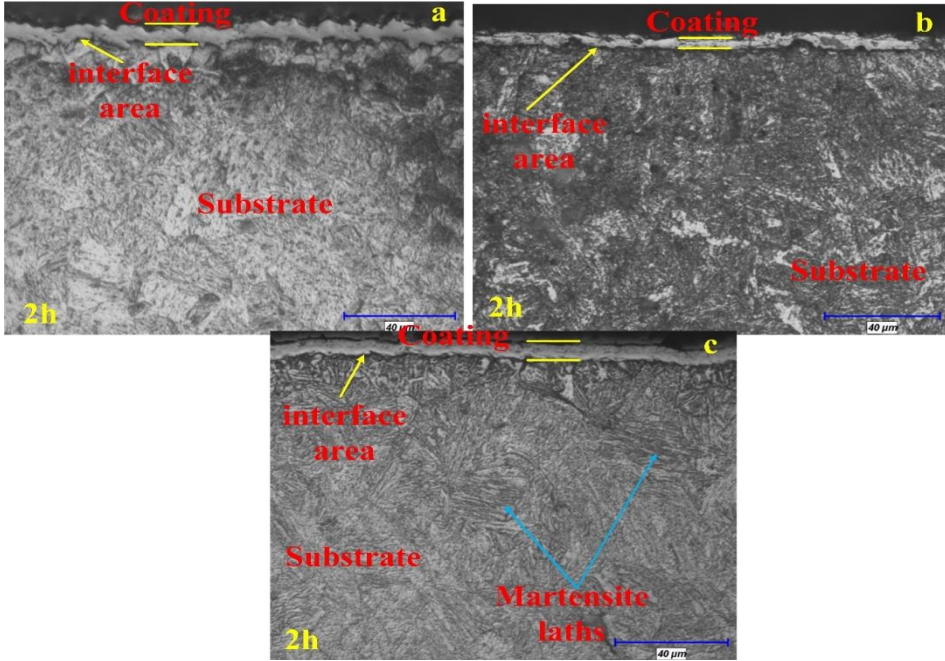


Figure 3. Microstructure of samples coated at 2 hours and a) 950 °C, b) 1000 °C, c) 1050 °C temperatures.

Figure 4 shows the graph of average coating thicknesses for the samples. The coating thickness increased with higher temperature and processing time, indicating improved diffusion. The variations in process temperature and duration significantly affected the thickness of the coating layer. In the TRD method, composition, substrate material, treatment duration, and temperature are all critical factors influencing the thickness of the coating layer formed on the surface [31]. Bülent et al. reported that in their titanizing process, the coating layer thickness varied between 2.19–14.72 μm and 3.65–26.5 μm depending on the process parameters, and that the coating was limited by the diffusion of interstitial atoms (C) from the substrate to the surface [8]. In this study, the average coating thicknesses measured at 950 °C for 1, 2, and 3 hours were 2.591 μm , 5.469 μm , and 7.79 μm , respectively. At 1000 °C, the thicknesses were 3.492 μm , 6.865 μm , and 8.212 μm , while at 1050 °C, they were 5.381 μm , 7.731 μm ,

and 9.148 μm for the same durations. It is noteworthy that coating thickness consistently increased with rising temperature and processing time [32-39].

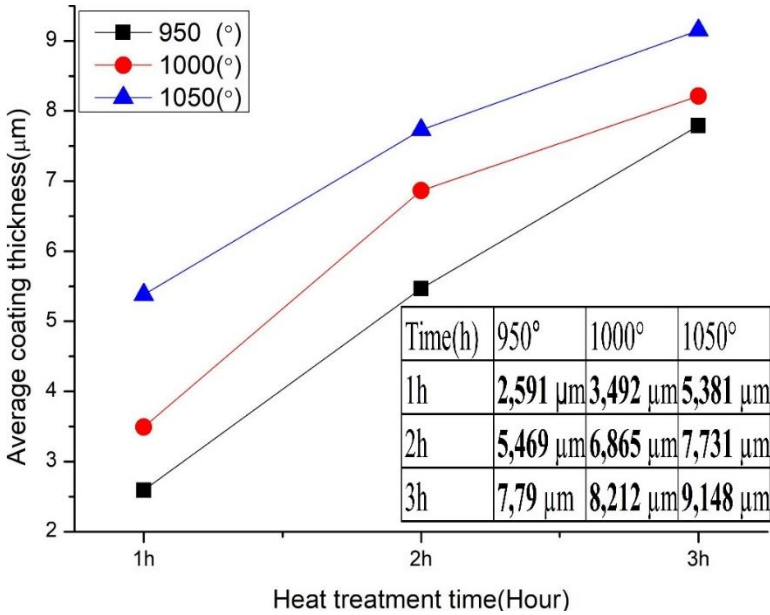


Figure 4. Average coating thicknesses of coated samples

2.2. SEM-EDS Analysis

Figure 5 displays the cross-sectional SEM-EDS images of the samples coated using the Thermo-Reactive Deposition (TRD) method at 950 °C, 1000 °C, and 1050 °C for 3 hours. Corresponding average elemental distributions and mapping images are presented in Figure 6. The coating is composed of three distinct zones: the outer coating layer, the interfacial region, and the substrate. The morphology and quality of both the coating/substrate interface and the internal phase boundaries are critical in determining the coating’s mechanical performance. A well-defined and continuous interface is essential for adhesion, preventing delamination, and ensuring long-term stability under service conditions [32]. The coating layers produced under these conditions exhibit excellent structural integrity, with no visible cracks despite thermal stresses and phase transformations during cooling. The interfaces are smooth, clean, and the coating thickness appears uniform across the cross-section [33]. Microstructural analysis revealed a martensitic structure within the coating layers. Elemental mapping confirms a high concentration of titanium (Ti) in the outer coating layer, while α -Fe content increases progressively toward the substrate. Ti content shows a sharp decline from the coating to the substrate, whereas carbon (C) decreases more

gradually, indicating significant interdiffusion of elements during the TRD process. Specifically, carbon tends to diffuse outward while Ti diffuses inward [28]. In the sample coated at 950 °C, strong metallurgical bonding was observed between the coating and substrate, although some pore-like features appeared at isolated surface locations. EDS analysis of this sample showed atomic percentages as follows: Ti: 64%, 72.4%, 23.2%, absent in the substrate C: 10.7%, 25.2%, 24.1%, 9.7%, 13.4%, Fe: 25.3%, 2.3%, 52.3%, 89.1%, 86.1% For the 1000 °C sample, EDS results were: Ti: 82.3%, 74.5%, 9%, 1.2%, C: 15.9%, 23.4%, 26.7%, 11.4%, 15%, Fe: 1.8%, 2.1%, 63.9%, 87%, 84.5%, In the 1050 °C sample, elemental distribution was as follows: Ti: 67.6%, 71.1%, 38.9%, 0.5%, C: 30.7%, 26.7%, 18.6%, 18.2%, 16%, Fe: 1.7%, 2.2%, 42.5%, 80.3%, 83.5%. These results clearly demonstrate high concentrations of Ti and C within the coating layers, while the substrate primarily contains Fe along with a minor amount of C. Increasing the process temperature and duration enhances elemental diffusion, facilitating deeper penetration of Ti and outward diffusion of C [20]. However, as the coating thickens, the diffusion of Fe toward the outer surface diminishes, resulting in a reduction of Fe content within the coating layer [34]. The presence of comparable amounts of Ti, Fe, and C in the interfacial region suggests the formation of a solid solution and metallurgical bonding due to atomic-scale interdiffusion. This transitional zone acts as a buffer layer, mitigating the thermal expansion mismatch between the coating and substrate, thereby improving interface strength and durability [35]. According to Figure 6, the average EDS values across all samples indicate an increase in Ti content with temperature, with the highest Ti concentration observed in the sample processed at 1050 °C for 1 hour. Elemental mapping for the 3-hour samples reveals dense distributions of Ti and C throughout the coating layers, while Fe appears in a dispersed, mist-like pattern, indicating a significantly lower presence in the outer layers [20].

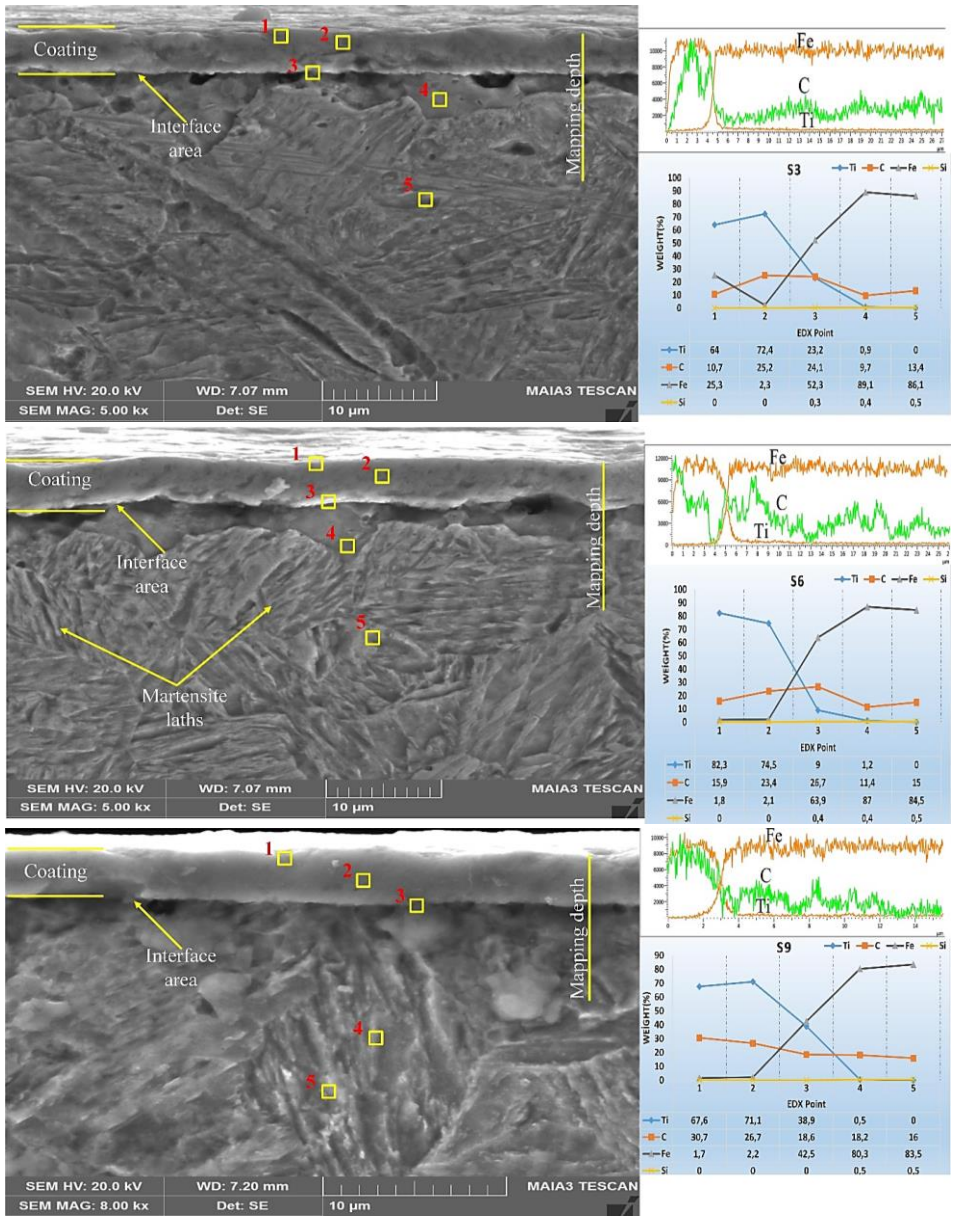


Figure 5. SEM-EDS images of samples coated at 950 °C, 1000 °C and 1050 °C for 3 hours.

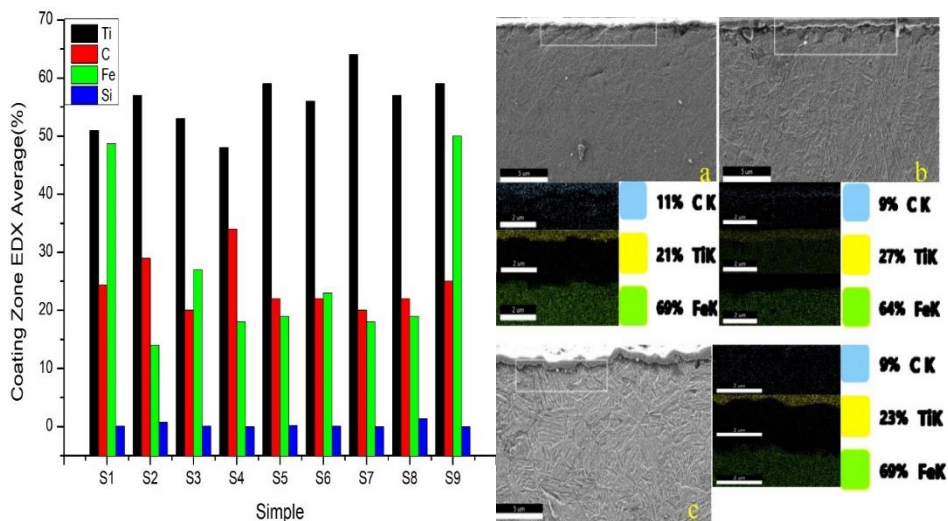


Figure 6. Average edx - temperature time graph of all samples and mapping image of samples coated at a) 950 °C; b) 1000 °C; c) 1050 °C heat treatment for 3 hours

2.3. XRD Analysis

Figure 7 presents the phase composition of the coating layers as determined by X-ray diffraction (XRD) analysis. The diffraction patterns reveal the presence of TiC, TiO₂, and α -Fe phases within the coating. Among these, TiC exhibits the most prominent peaks, indicating its dominant presence in the coating layer. This high-intensity TiC formation is primarily attributed to the higher diffusion rate of Ti atoms compared to carbon atoms. As carbon atoms, which are plentiful at the surface, diffuse into the Ti lattice and occupy vacant sites, the formation of TiC is significantly promoted [32]. The tendency for Ti to form carbides is further supported by its limited solid solubility in α -Fe, coupled with the high and uniform carbon concentration present on the substrate surface at the onset of the coating process. These conditions strongly favor the nucleation and growth of TiC phases [40-48]. It is well-established that the presence of carbide structures, along with martensitic phases in steels, contributes to enhanced hardness and improved wear resistance [49]. This interpretation aligns with the EDS findings shown in Figures 5 and 6, which demonstrate elevated concentrations of both Ti and C in the coating region. These elemental distributions further support the inference that a dense TiC phase has been successfully synthesized during the coating process [50-52].

In correlation with phase formation, Figure 8 illustrates the microhardness profile across the cross-section of the coated samples. A clear gradient is observed, with hardness values progressively decreasing from the coating layer toward the substrate. This gradient confirms the presence of hard carbide phases—most notably TiC—in the outer layer. These findings are consistent with previous research in the field, confirming the reliability of the results and their agreement with reported literature data [53-55].

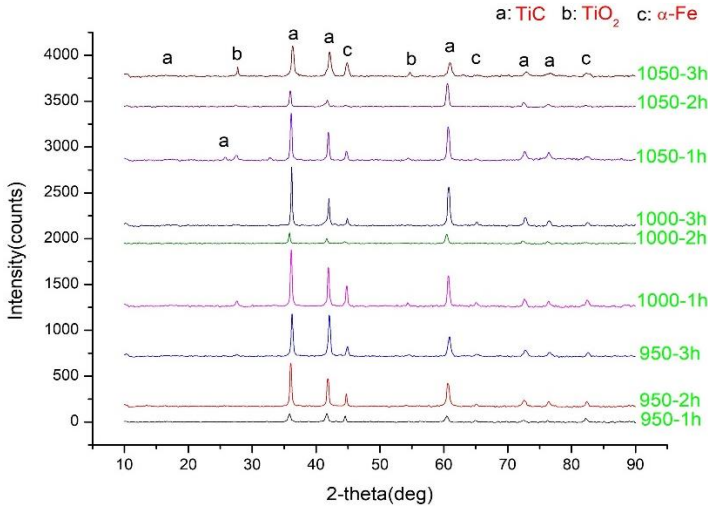


Figure 7. XRD results of coatings

2.4. Microhardness Analysis

The graph of microhardness measurements is presented in Figure 8. Hardness values varied notably with changes in temperature and duration. The maximum hardness, measured at 3036 HV0.5, was obtained from the coating sample that underwent heat treatment at 1050°C for 3 hours. This high hardness is mainly attributed to the secondary phase strengthening effect of the hard TiC phase, which, due to its high volume fraction, effectively restricts dislocation motion under applied load [56,57]. In contrast, the lowest hardness value, 482 HV0.5, was recorded in the substrate region of the sample coated at 950°C for 1 hour. The decrease in hardness from the coating layer toward the substrate is primarily due to the influence of the phases formed in the coating layer. Figure 9 illustrates how average microhardness values change with temperature and duration. Zhao et al. conducted a study on B4C-TiC-Ni composite coatings produced by a laser method and found that an increase in TiC content within the coating region correlated with higher hardness, reporting a microhardness of 1339.7 HV0.5 [41].

Similar findings have been reported in previous studies on TiC coatings produced by various methods [42, 43].

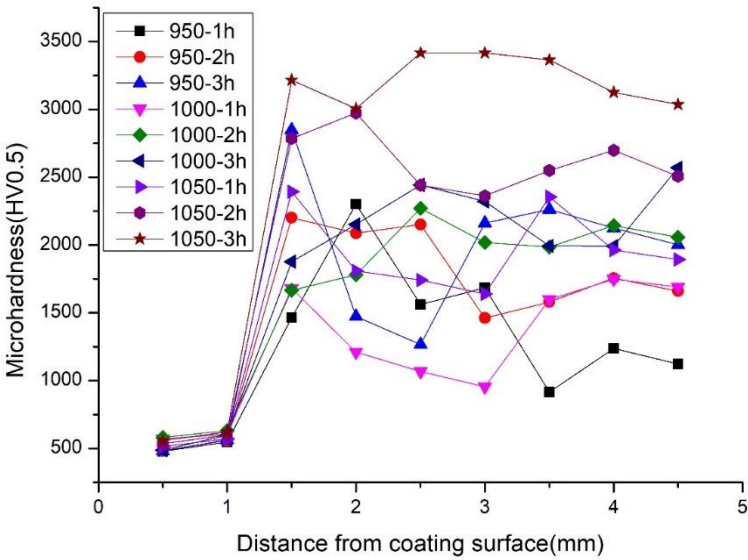


Figure 8. Microhardness graph of coatings

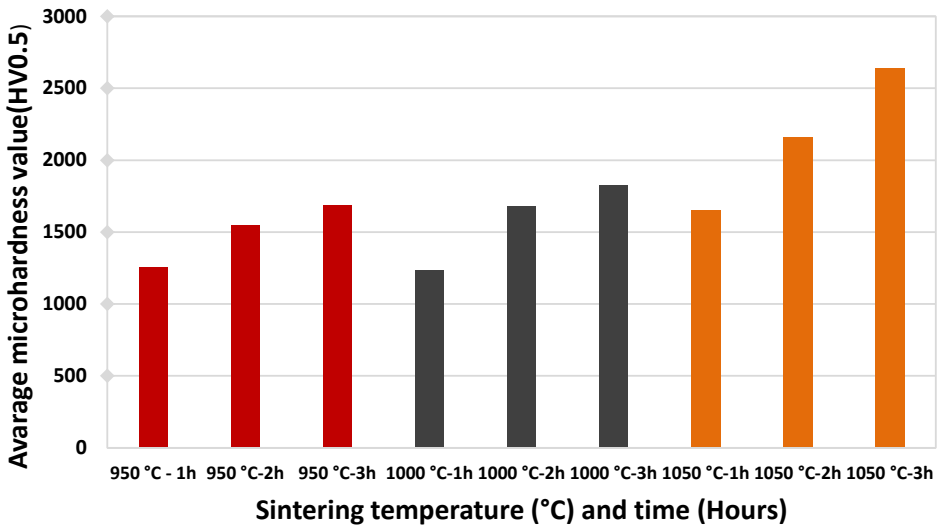


Figure 9. Microhardness change graph depending on temperature and time

2.5. Wear Analysis

The results from the wear tests evaluating the surface wear resistance of the coatings are displayed in Figures 10a and 10b. Figure 10a depicts how the

coefficient of friction (COF) changes over time, while Figure 10b presents both the average COF and average microhardness values. Notably, the COF for the sample treated at 1050°C for 3 hours showed a considerable rise from 0.2 to 0.4 throughout the test duration. Initially, the presence of hard structures led to a lower friction coefficient. However, as the outer hard layer wore off, the COF behavior stabilized. According to Yahya et al., during wear testing, the interaction between the surface and abrasive particles decreases the contact area, thus reducing shear wear [44]. Similarly, Steel and Kilickap emphasized that the presence of hard particles boosts a material's hardness and enhances its tribological performance [45]. Among all samples, the one treated at 1050°C for 3 hours demonstrated the lowest COF, whereas the untreated base material showed the highest COF, reaching up to approximately 0.9. A comparison among coated samples revealed that the COF decreased with higher treatment temperatures and longer durations. The graph plotting average COF against microhardness indicates an inverse relationship: as microhardness increases, COF decreases. Therefore, microhardness is considered a major factor affecting friction. Coatings combining low COF with high hardness exhibited superior wear resistance, suggesting that both friction coefficient and hardness are critical indicators of wear resistance in such tests [57].

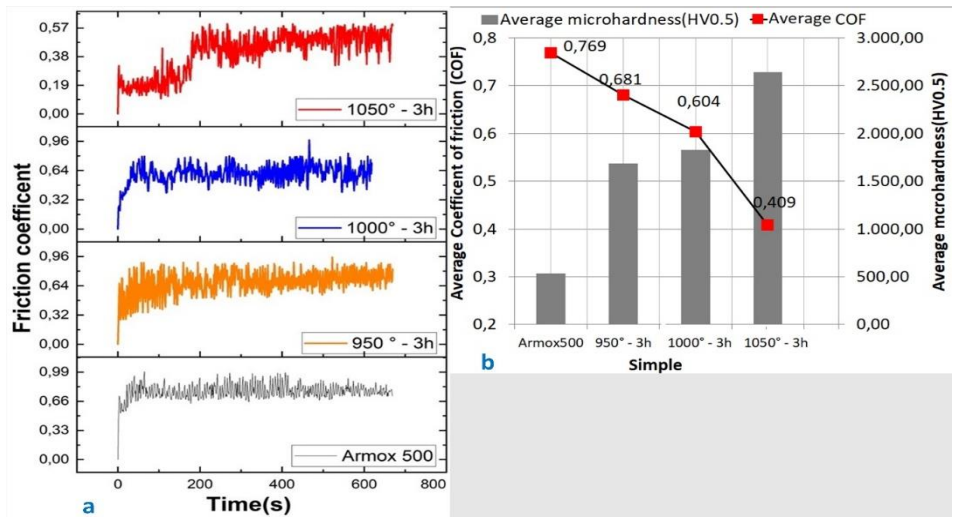


Figure 10. Wear graph of the coatings (a) and average microhardness and average COF graph (b)

3. GENERAL RESULTS

TiC coatings were applied to the surface of Armox 500 steel via the Thermo-Reactive Diffusion (TRD) process. The coatings were formed at three distinct temperatures (950°C, 1000°C, and 1050°C) and for three different durations (1, 2, and 3 hours). Microstructural features and surface hardness were examined as functions of these parameters to identify the most effective treatment conditions. A summary of the findings is provided below:

1. The TRD technique was used to successfully coat the Armox 500 steel surface. The coatings showed no signs of porosity or cracking. The coating layer and the substrate formed a metallurgical connection.
2. EDS analysis showed that the coating layer contained high concentrations of Ti and C, while the substrate mainly consisted of high Fe content with a small amount of C. The presence of Ti, C, and Fe in the interface layer indicates successful diffusion.
3. TiC, TiO₂, and α -Fe phases were formed in the coating layer. TiC phase exhibited high intensity peaks in the coating region, which is mainly attributed to the higher diffusion rate of Ti atoms compared to carbon atoms.
4. The coating sample that was heated to 1050 °C for three hours had the greatest hardness value, 3036 HV0.5. The substrate area of the sample coated at 950 °C for one hour had the lowest hardness, 482 HV0.5. Phases that occur in the coating region are the main cause of the hardness drop from the coating layer toward the substrate.
5. The average coating thicknesses formed on the surface depending on temperature and time were measured as follows: at 950 °C for 1, 2, and 3 hours; 2.591 μm , 5.469 μm , and 7.79 μm , respectively; at 1000 °C for 1, 2, and 3 hours; 3.492 μm , 6.865 μm , and 8.212 μm , respectively; and at 1050 °C for 1, 2, and 3 hours; 5.381 μm , 7.731 μm , and 9.148 μm , respectively. The coating thickness continued to increase with rising temperature and time.
6. When compared to the untreated substrate, the coated samples exhibited a greater degree of wear resistance. The sample coated at 1050 °C for three hours had a friction coefficient of about 0.3, whereas the base material had a coefficient of about 0.9. This finding showed that when temperature and duration increased, microhardness increased and the friction coefficient decreased.

REFERENCES

1. Khare, S., Kumar, K., Choudhary, S., Singh, P. K., Verma, R. K., & Mahajan, P. (2023). Material Characterization of Armor Steel and Investigation of Its Ballistic Performance. *Journal of Materials Engineering and Performance*, 32(15), 6833-6849.
2. Saxena, A., Kumaraswamy, A., Kotkunde, N., & Suresh, K. (2019). Constitutive modeling of high-temperature flow stress of armor steel in ballistic applications: a comparative study. *Journal of Materials Engineering and Performance*, 28, 6505-6513.
3. Barényi, I., Majerík, J., Bezečný, J., Krbařa, M., Sedlák, J., & Jaroř, A. (2019). Material and Technological Aspects while Processing of Selected Ultra High Strength Steel. *Manuf. Technol*, 19, 184-189.
4. Saxena, A., Kumaraswamy, A., Madhu, V., & Madhusudhan Reddy, G. (2018). Study of tribological characteristics of multi-pass SMAW armox 500T steel joints. *Journal of Materials Engineering and Performance*, 27, 4300-4307.
5. Altuncu, E. (2019). Laser cladding of martensitic stainless steels on armor steels. *Emerging Materials Research*, 9(1), 55-58.
6. Akkař, M., & Grdal, M. (2025). Effect on Machinability Characteristics of Cryogenic Process and Performance Assessment by Using Machine Learning Approach with Scaled Conjugate Gradient Algorithm. *Iranian Journal of Science and Technology, Transactions of Mechanical Engineering*, 1-20.
7. Youssef, M., El-Shenawy, E. H., Khair-Eldeen, W., Adachi, T., Nofal, A., & Hassan, M. A. (2023). The Influences of Nb Microalloying and Grain Refinement Thermal Cycling on Microstructure and Tribological Properties of Armox 500T. *Materials*, 16(23), 7485.
8. Castillejo, F., Marulanda, D., Rodrguez, O., & Olaya, J. (2011). Electrical furnace for producing carbide coatings using the thermoreactive deposition/diffusion technique. *Dyna*, 78(170), 192-197.
9. Kurt, B., zdođan, L., Gney, B., Blkbařı, . S., & Gnen, A. (2020). Characterization and wear behavior of TiBC coatings formed by thermoreactive diffusion technique on AISI D6 steel. *Surface and Coatings Technology*, 385, 125332.
10. Wang, M., Li, Y., Jin, T. & Fu, H. (2024). Wear resistance optimized by heat treatment of an *in-situ* TiC strengthened AlCoCrFeNi laser cladding coating. *Materials Testing*, 66(8), 1168-1182.

11. Akkaş, M. (2024). The effect of molten salt on the mechanical properties and microstructure of CuNiSi alloys with reinforced Fe. *Science of Sintering*, (00), 28-28.
12. Kılıç, M., Gök, S., & Adıyaman, O. (2024). TiC-C İle Kaplanan AISI 1040 Çelik Yüzeyinin Aşınma Özelliklerinin İncelenmesi. *Yüzüncü Yıl Üniversitesi Fen Bilimleri Enstitüsü Dergisi*, 29(1), 275-291.
13. Islak, S., Kır, D., Buztoy, S., Özorak, C., Akkaş, M., Çalığülü, U., & Yıldırım, M. M. (2015). Microstructure characterization of WCCo-Mo based coatings produced using high velocity oxygen fuel. *Pamukkale Üniversitesi Mühendislik Bilimleri Dergisi*, 21(8), 344-347.
14. Gultekin T. & Tekiner, Z. (2021). Comparison between acidic electroless deposited Cu, Ni coating and a physical vapor deposited (PVD) Al coating on an acrylonitrile– butadiene–styrene (ABS) substrate. *Materials Testing*, 63(10), 950-955.
15. Beltir, Y.M., Imak, A., Kirik, I., Turgut, A. & Koc, V. (2025). Microstructure and wear properties of NiTi–XSiC coating of AISI 1020 by SHS" *Materials Testing*, 67(2), 386-396.
16. Kilic, M. (2020). TiC coatings on an alloyed steel produced by thermal diffusion. *Materials Testing*, 62(9), 909-912.
17. Aghaie-Khafri, M., & Fazlalipour, F. (2008). Vanadium carbide coatings on die steel deposited by the thermo-reactive diffusion technique. *Journal of Physics and Chemistry of Solids*, 69(10), 2465-2470.
18. Islak, S., Özorak, C., Sezgin, C. T., & Akkaş, M. (2016). Trd Yöntemiyle Supap Çeliği Yüzeyinde Üretilen Kaplamaların Mikroyapı Ve Aşınma Özellikleri. *Technological Applied Sciences*, 11(3), 75-85.
19. Soltani, R., Sohi, M. H., Ansari, M., Haghighi, A., Ghasemi, H. M., & Haftlang, F. (2017). Evaluation of niobium carbide coatings produced on AISI L2 steel via thermo-reactive diffusion technique. *Vacuum*, 146, 44-51.
20. Günen, A., Soylu, B., & Karakaş, Ö. (2022). Titanium carbide coating to improve surface characteristic, wear and corrosion resistance of spheroidal graphite cast irons. *Surface and Coatings Technology*, 437, 128280.
21. Sen, U. (2005). Wear properties of niobium carbide coatings performed by pack method on AISI 1040 steel. *Thin Solid Films*, 483(1-2), 152-157.
22. Buytoz, S., & Yılmaz, B. (2019). Investigation of microstructural properties of TiC coating obtained by termoreactive diffusion process on AISI4140 steel. *Firat University Journal of Engineering Sciences*, 31, 473-480.

23. Akkaş, M., K TABONAH, T. M., A ELFGHI, A. M., & Özorak, C. (2023). POWDER METALLURGICAL FABRICATION OF CO REINFORCED CUNISI MATRIX COMPOSITES: MICROSTRUCTURAL AND CORROSION CHARACTERIZATION. *Technological Applied Sciences*, 18(4), 64-74.
24. Günen, A., Kurt, B., Milner, P., & Gök, M. S. (2019). Properties and tribological performance of ceramic-base chromium and vanadium carbide composite coatings. *International Journal of Refractory Metals and Hard Materials*, 81, 333-344.
25. Ghadi, A., Ebrahimnezhad-Khaljiri, H., & Gholizadeh, R. (2023). A comprehensive review on the carbide-base coatings produced by thermo-reactive diffusion: microstructure and properties viewpoints. *Journal of Alloys and Compounds*, 171839.
26. Özorak, C., Tabonah, T. M. K., & Akkaş, M. (2023). Production of CuNiSi Composites by Powder Metallurgy Method: Effects of Ti on the microstructural and corrosion properties. *European Journal of Technique (EJT)*, 13(2), 88-93.
27. Fan, X. S., Yang, Z. G., Zhang, C., & Zhang, Y. D. (2012). Thermo-reactive deposition processed vanadium carbide coating: growth kinetics model and diffusion mechanism. *Surface and Coatings Technology*, 208, 80-86.
28. Pouraliakbar, H., Khalaj, G., Gomidželović, L., Khalaj, M. J., & Nazerfakhari, M. (2015). Duplex ceramic coating produced by low temperature thermo-reactive deposition and diffusion on the cold work tool steel substrate: Thermodynamics, kinetics and modeling. *Ceramics International*, 41(8), 9350-9360.
29. Kurt, B., Günen, A., Kanca, Y., Koç, V., Gök, M. S., Kırar, E., & Askerov, K. (2018). Properties and tribologic behavior of titanium carbide coatings on AISI D2 steel deposited by thermoreactive diffusion. *Jom*, 70(11), 2650-2659.
30. Akkaş, M. (2022). Synthesis and characterization of MoSi₂ particle reinforced AlCuMg composites by molten salt shielded method. *Türk Doğa ve Fen Dergisi*, 11(4), 11-17.
31. Efe, Gozde Celebi, Yener, Tuba, Ozcelik, Gamze and Ozkan, Hidayet. "TiB-based coating formation on Ti6Al4V alloy" *Materials Testing*, vol. 66, no. 12, 2024, pp. 1965-1971.
32. Topuz, A., Karaaslan, A., & Topuz, P. (2007). Chromium Carbide Coating of Hot Work Tool Steel X40CrMoV51 and Nitriding Steel 34CrAlNi7 by

- a Thermoreactive Diffusion Process. *Materials Testing*, 49(11-12), 606-608.
33. Xiao, L., Li, S., Xu, J., Zhao, Z., Xiang, H., Bao, X., ... & Liu, S. (2020). Failure mechanism and improvement process of preparing carbide coating on high speed steel by thermal diffusion reaction. *Surface and Coatings Technology*, 404, 126398.
 34. Akkaş, M., & Elfgħi, A. M. A. (2022). TiB₂ parçacık takviyeli alümin kompozitlerin üretilebilirliğinin araştırılması. *Uluslararası Doğu Anadolu Fen Mühendislik ve Tasarım Dergisi*, 4(2), 118-128.
 35. Zhang, J., Li, S., Lu, C., Sun, C., Pu, S., Xue, Q., ... & Huang, M. (2019). Anti-wear titanium carbide coating on low-carbon steel by thermo-reactive diffusion. *Surface and Coatings Technology*, 364, 265-272.
 36. Wang, M., Li, Y., Jin, T., & Fu, H. (2024). Wear resistance optimized by heat treatment of an in-situ TiC strengthened AlCoCrFeNi laser cladding coating. *Materials Testing*, (0)
 37. Pazarlıođlu, S. S., Kon, Ö., & Şen, Ş. (2012). Niobium boride coating on the surface of AISI 1010 by a duplex treatment. *Usak University Journal of Material Sciences*, 1(2), 199-204.
 38. Caligulu, U., Durmus, H., Akkas, M., & Sahin, B. (2021). Microstructure and mechanical properties of Ni matrix B₄C reinforced functionally graded composites. *Science of Sintering*, 53(4), 475-484.
 39. Bai, H., Kang, L., Zhang, P., Bai, J., Liu, J., Cao, B., & Xu, Y. (2023). TiC-Fe gradient coating with high hardness and interfacial adhesion strength on cast iron prepared by in-situ solid-phase diffusion method. *Vacuum*, 215, 112336.
 40. Biesuz, M., & Sglavo, V. M. (2016). Chromium and vanadium carbide and nitride coatings obtained by TRD techniques on UNI 42CrMoS4 (AISI 4140) steel. *Surface and Coatings Technology*, 286, 319-326.
 41. Sun, C., Xue, Q., Zhang, J., Wan, S., Tieu, A. K., & Tran, B. H. (2018). Growth behavior and mechanical properties of Cr-V composite surface layer on AISI D3 steel by thermal reactive deposition. *Vacuum*, 148, 158-167.
 42. Ganji, O., Sajjadi, S. A., Yang, Z. G., & Mirjalili, M. (2022). Tribological properties of duplex coatings of chromium-vanadium carbide produced by thermo-reactive diffusion (TRD). *Ceramics International*, 48(6), 7475-7490.
 43. Akamatsu, S., Hasebe, M., Senuma, T., Matsumura, Y., & Kisue, O. (1994). Thermodynamic calculation of solute carbon and nitrogen in Nb and Ti added extra-low carbon steels. *ISIJ international*, 34(1), 9-16.

44. Akkaş, M., & Al, S. F. R. A. (2021). Effect of hot pressing and reinforcement of TiC and WC on the mechanical properties and microstructure of AlCuFeCrNi HEAs alloy. *Science of Sintering*, 53(1), 19-35.
45. Çakir, M. V. (2022). A Comparative Study on Tribocorrosion Wear Behavior of Boride and Vanadium Carbide Coatings Produced by TRD on AISI D2 Steel. *Protection of Metals and Physical Chemistry of Surfaces*, 58(3), 562-573.
46. Jam, A., Nikzad, L., & Razavi, M. (2017). TiC-based cermet prepared by high-energy ball-milling and reactive spark plasma sintering. *Ceramics International*, 43(2), 2448-2455.
47. Bai, H., Zhong, L., Shang, Z., Cui, P., Kang, L., Lv, Z., & Xu, Y. (2020). Microstructure and fracture toughness of compact TiC-Fe gradient coating fabricated on cast iron substrate by two-step in situ reaction. *Jom*, 72, 2154-2163.
48. Akkaş, M. (2021). Production and characterization of boron carbide and silicon carbide reinforced copper-nickel composites by powder metallurgy method. *Materialwissenschaft und Werkstofftechnik*, 52(1), 32-42.
49. Kumar, S., & Singh, A. P. (2024). Characterization of surface properties of TiC ceramic coating developed on AISI 1020 steel. *Surfaces and Interfaces*, 46, 103960.
50. Zhao, Y., Yu, T., Sun, J., & Jiang, S. (2020). Microstructure and properties of laser cladded B4C/TiC/Ni-based composite coating. *International Journal of Refractory Metals and Hard Materials*, 86, 105112.
51. Naem, M., Díaz-Guillén, J. C., de Sousa, E. M., Monção, R. M., Bandeira, R. M., Junior, C. A. A., ... & de Sousa, R. R. M. (2024). Improved surface properties of AISI-420 steel by TiC based coating using graphite cathodic cage with titanium lid in plasma deposition. *Surface and Coatings Technology*, 477, 130406.
52. Yoshida, K., Takishima, N., & Kawakami, M. (1989). TiC-Coating on the high carbon steels SK3 and SKS93 using the powder-pack method. *High Temperature Materials and Processes*, 8(4), 191-200
53. Çelik, Y.H., Seçilmiş, K. (2017). Investigation of wear behaviours of Al matrix composites reinforced with different B4C rate produced by powder metallurgy method, *Advanced Powder Technology*, 28, 2218–2224.
54. Akkaş, M. (2020). The mechanical and corrosion properties of WCCo–Al coatings formed on AA2024 using the HVOF method. *Materials Research Express*, 7(7), 076515.

55. Çelik H.Y., Erol, K. (2019). Hardness and wear behaviours of Al matrix composites and hybrid composites reinforced with B4C and SiC. *Powder Metallurgy and Metal Ceramics*, 57(9-10), 613-622.
56. Kilic, M., Imak, A., & Kirik, I. (2021). Surface modification of AISI 304 stainless steel with NiBSi-SiC composite by TIG method. *Journal of Materials Engineering and Performance*, 30(2), 1411-1419.
57. Em Akra, K. M., Akkaş, M., Boz, M. U. S. T. A. F. A., & Seabra, E. (2020). The production of AZ31 alloys by gas atomization method and its characteristics. *Russian Journal of Non-Ferrous Metals*, 61, 332-345.

Chapter 2

PRODUCTION and FRICTION PROPERTIES of Al, Mg and Ti ALLOY CARBIDE REINFORCED COMPOSITES USING POWDER METALLURGY-A REVIEW

İhsan KIRIK¹

¹ Prof. Dr., Department of Machinery and Metal Technologies, Bingol University, Turkey,
ikirik@bingol.edu.tr, (ORCID: 0000-0002-8361-319X)

1. INTRODUCTION

With the rapid development in technology, existing materials alone are insufficient to meet the desired needs. From this perspective, the development activities of the production properties of alloy and composite materials, which are among the important materials of our age, continue to increase. Composite materials (CMs) are indispensable for automotive, marine vehicles, defense industry and space vehicles. The ability to use these materials especially at high temperatures and their volumetric stability are among the factors that increase their use. [1] Composites are produced by dispersing different phases in a matrix. Since the reinforcement phase generally has better properties than the continuous phase is called the matrix [2-4]. The matrix phase provides the formal integrity of the CMs and the reinforcement materials are used to provide the desired properties. The widespread use of composite materials makes them inevitable due to the reasons underlying them (high strength, flexibility, fracture toughness, fatigue and wear, etc.). We can divide composite materials into three main classes: polymer, metal and ceramic matrix composites. Metal matrix composites (MMCs) can be made using a variety of techniques using solid and liquid state processes. Powder metallurgy (PM) is commonly used production methods [5]. PM is the process of producing metal or ceramic powders and combining these powders with mechanical and thermal effects to form a product. The relatively low processing temperature, which prevents strong reinforcement/matrix interface reactions and minimizes undesirable reactions between the matrix/reinforcement, close to net shaped production and the most uniform allocation of reinforcement content in the matrix are the greatest advantages. Usage rates of metal matrix materials used by industrial companies is seen in picture 1 [6-7]. Metals like Al, Cu, Ti, Ni, Mg, Zn and their alloys are utilized as matrix materials in the creation of metal matrix composite materials, whereas elements like TiC, SiC, B₄C, and Al₂O₃ are utilized as reinforcements.

2. ALUMINIUM and ITS ALLOYS

Aluminum is widely used in metal matrix composites due to its important properties such as being abundant in nature, easy to process, lightness, good corrosion resistance and reinforcing.

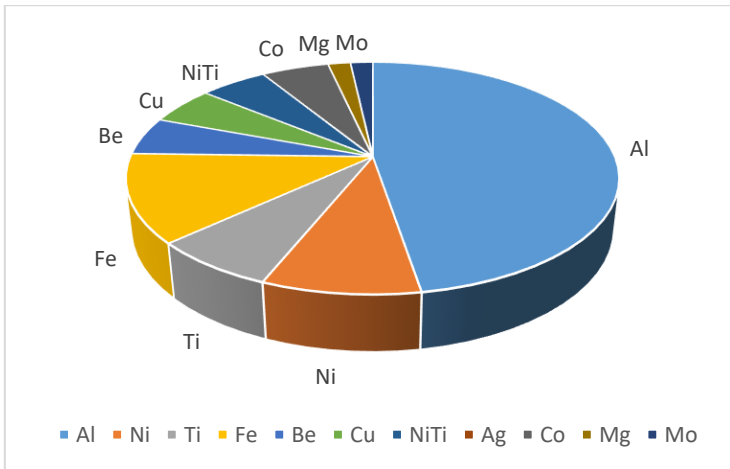


Figure 1. Usage rates of MMCs used by industrial companies [4].

Aluminum is widely used in metal matrix composites due to its important properties such as being abundant in nature as seen in Figure 2, easy to process, lightness, good corrosion resistance and reinforcing. Al is a ductile, soft, non-magnetic, silvery-white metal. It is a light metal with a melting temperature of 658 degrees and a specific gravity of 2.7. Al's tensile strength ranges from 90 to 150 MPa [8-10].

The properties of Al are listed as follows:

- ✓ **Formability:** In addition to being appropriate for extrusion, aluminum can be bent and rolled in both hot and cold temperatures.
- ✓ **Machining:** The majority of machining techniques, including as milling, drilling, punching, cutting, bending, etc., can be used to easily deal with aluminum.
- ✓ **Weight:** Aluminum has a density of 2.7 grams per cubic centimeter, or roughly one-third that of steel.
- ✓ **Strength:** The tensile strength of aluminum alloys ranges from 70 to 700 MPa. The most common alloys for extrusion are 150–300 MPa.
- ✓ **Joining:** There are several methods for joining aluminum, including cold welding by forcing profiles together, bonding, welding (MIG, TIG, and Friction Stir Welding), and taping.
- ✓ **Conductivity:** Aluminum is an excellent heat and electrical conductor. With the same conductivity, an aluminum conductor weighs roughly half as much as a copper conductor.
- ✓ **Reflectivity:** Heat radiation and visible light are both well-reflected by aluminum.

- ✓ **Non-magnetic material:** Aluminum is a paramagnetic, or non-magnetic, substance. Aluminum is frequently used in magnet X-ray equipment to prevent magnetic field interference.
- ✓ **Economical:** It is abundant compared to other matrix metals and therefore a relatively cheap material.

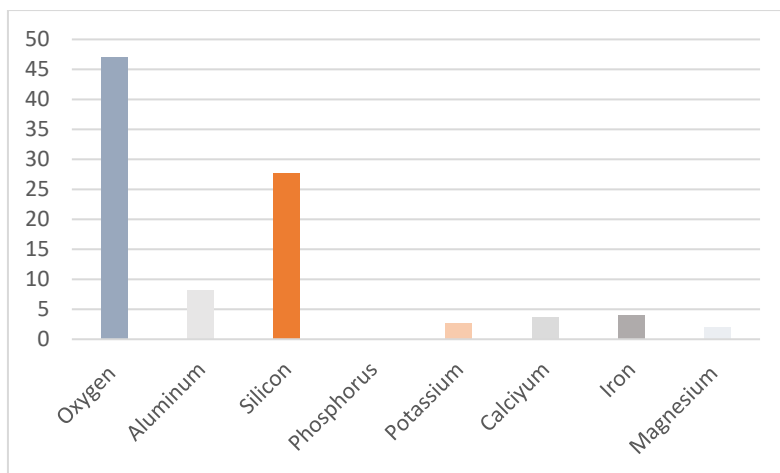


Figure 2. The amounts of elements found in the Earth's crust

3. MAGNESIUM and ITS ALLOYS

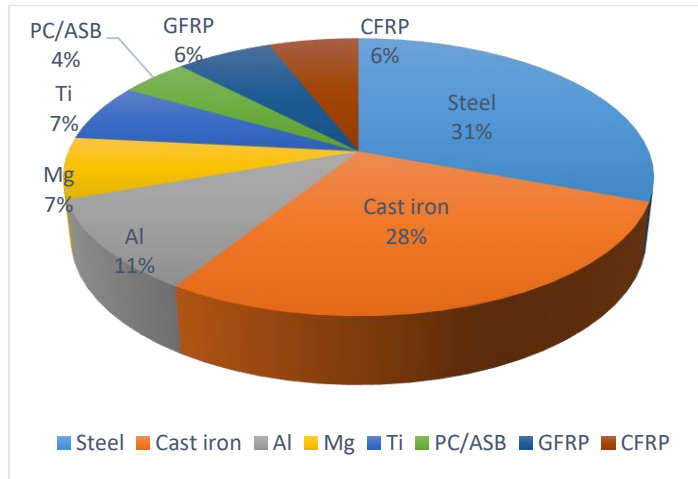
It is expected that the usage areas of magnesium alloys, which are light metal alloys, in industrial applications will become quite widespread in the future and accordingly the usage of magnesium-based composite materials will increase. Magnesium alloys have special importance in the defense industry and automotive sector due to their properties such as lightness and high specific strength [1-10]. They are generally not preferred for use without alloys because they have low strength and toughness values. For this reason, they are used by alloying. Magnesium and its alloys also have high thermal conductivity, good electromagnetic protection, high dimensional stability, high damping, good processability and easy recycling properties [9-17].

Mg and its alloys are coded as two letters, two or three digit numbers, respectively [18]. They can reduce the weight of automobiles to a great extent without compromising structural properties. The effects of magnesium alloying elements are as follows; Al increases strength; Zn increases toughness; Mn increases resistance to corrosion. However, an increase in the amount of Zn causes hot brittleness [19]. Corrosion creep is the term used to describe the combined impact of stress and corrosion on the viscoelastic behavior of

magnesium alloys [20-25]. The structure is extremely vulnerable to corrosion creep due to the Al concentration [26].

The properties of Mg are listed as follows:

- ✓ **Formability:** The majority of magnesium applications are met by AZ91, a die-casting and pressure-casting alloy. In general, it is interesting that magnesium can be formed by forging, as opposed to pressure casting, which is currently commonly employed [27]. To increase the shaping ability of sheet metal, which is poor at room temperature, new techniques are being developed and tested [28, 29].
- ✓ **Machining:** Magnesium can be readily worked with using most machining techniques, such as milling, drilling, punching, cutting, etc.
- ✓ **Weight:** About the Element Magnesium With a density of 1.7g/cm^3 (Figure 3) (106.13lb/ft^3) at 20°C (68°F), it is the least dense of the structural metals. It is 33% lighter than Al and 77% lighter than steel.
- ✓ **Strength:** In addition to the lightness of Mg and its alloys, we also see that some of its alloys can exhibit tensile strength values around 300-350 MPa, at a level that can compete with gray cast iron.
- ✓ **Jointing:** Most magnesium alloys can be welded using MIG, TIG and other friction joining processes and weldability requires special conditions.
- ✓ **Conductivity:** High coefficient of thermal expansion ($25.5 \times 10^{-6} \text{ m/m}^\circ\text{C}$), High thermal conductivity (approximately 150 W/mK), Relatively high electrical conductivity (approximately 40% of copper).
- ✓ **Reflectivity:** Mg reflects visible light and heat radiation well.
- ✓ **Non-magnetic material:** Magnesium is a paramagnetic, or non-magnetic.
- ✓ **Economical:** More than 85% of the world's primary magnesium production, that is, approximately 800,000 tons of the 1,200,000 tons annual production, is made by China. In a sense, China is a monopoly country in magnesium production, and the European Union and Japan meet 95% of their magnesium needs from China.



*PC/ASB: Polycarbonat ASB, GFRP: Glas fiber reinforced polimers
CFRP: Carbon fiber reinforced polimers*

Figure 3. Densities of materials [40].

In addition to these properties, the disadvantages of Mg and its alloys are as follows. Difficulty in cold forming, limited strength at high temperatures, high shrinkage rate during solidification, corrosion properties, metal production costs depending on the production method [30-39].

4. TITANIUM and ITS ALLOYS

Titanium and its alloys are commonly used as matrix materials in metal matrix composites. The thin layer of TiO₂ that develops on the surfaces of these materials gives them exceptional resistance to corrosion. Titanium and its alloys (Ni-Ti alloys) are also used as biomaterials because of their biocompatibility. Despite being quite expensive, this material is preferred in high temperature applications due to its incredibly low thermal expansion coefficient. They are beneficial in the aerospace and aviation industries due to their exceptional strength/specific gravity ratio. Titanium is a chemical element with the symbol Ti. Titanium alloys are usually made of about 88% Ti and the alloying elements, mostly vanadium (V) and aluminum (Al). Pure Titanium offers the best combination of good strength, formability and weldability. Titanium and its alloys are used in defense, space and aircraft industries, electrochemical industries, kitchen products, engine components, high temperature chemical production, marine applications [40-46].

The properties of Ti and its alloy are listed as follows:

- ✓ **Machining:** Titanium is an expensive and difficult material to machine. Although not as popular in machine shops as steel or aluminum, it is an important material to master due to its high material and manufacturing costs. Machinability varies between 15% and 45%.
- ✓ **Weight:** Titanium is a low-density element (approximately 60% less than iron) and can be strengthened by alloying and deformation processes. Its density is 4.51 g/cm².
- ✓ **Strength:** Commercially available, unalloyed titanium has a tensile strength between 275 and 590 MPa, which is mostly determined by its iron and oxygen contents. Strength increases with the amount of iron and oxygen present. Grades of titanium alloyed for commercial use can have strengths as low as 600 MPa (Ti-3Al-2.5V) to as high as 1250 MPa (Ti-15Mo-5Zr-3Al, a high strength alloy).
- ✓ **Joining:** The sensitivity of Ti and its alloys to gases limits the use of various welding methods and necessitates the adoption of a number of additional precautions [41-43].
- ✓ **Conductivity:** Titanium conducts heat very poorly. As a result, heat produced during the cut primarily moves to the cutting tool rather than the chips and the workpiece.
- ✓ **Formability:** Because of its great degree of flexibility, cutting forces can easily bend titanium.
- ✓ **Reflectivity:** The reflectivity of titanium alloys is comparable to that of steel and is likewise highly dependent on the laser wavelength.
- ✓ **Economical:** It accounts for 0.6% of production. Its share of titanium output is 0.25%, while it possesses 0.33% of the world's titanium deposits. It is anticipated that this rate will continue to rise. There are 820 million tons of metal titanium in the world, and there are 2 billion tons of proved and probable reserves [45-49].

5. POWDER METALLURGY'S REPORTED WORK on Al, Ti and Mg ALLOY COMPOSITES

Aluminum matrix composite materials (AMCs) have attracted significant attention and research due to their applications in various sectors such as aerospace, automotive, marine vessels and kitchenware. By adding carbide and oxide compounds to these composites, mechanical properties are improved and properties such as friction (hardness and wear) can be significantly increased. These ceramic materials (SiC, TiC, B₄C, Al₂O₃, MgO, etc.) incorporated into the matrix phase help to improve various properties such as strength, durability, wear,

hardness and heat resistance. Improved thermo-mechanical properties, sustainability, wear resistance and cost-effectiveness make these AMCs highly versatile. [50-52]. Al matrix composites produced by powder metallurgy, which is indispensable in industrial applications. They drew attention to reinforcement elements such as Al₂O₃, B₄C, SiC and MgO. As a result of their studies, they determined that carbides have higher strength properties, wear and hardness values compared to oxides. Based on these improved properties, it was determined that they could be preferred in high-performance applications such as industrial applications and cutting tools [53].

Singh stated in his study that composites formulated by combining aluminum and magnesium oxide (MgO) particles provide an optimum balance between lightweight structure and high strength-to-weight ratio. He stated that the main objective of his study is to conduct a comprehensive analysis of AMCs reinforced with MgO particles. The synthesis techniques, the mechanisms that strengthen the material, and a detailed investigation of how MgO reinforcement affects mechanical and wear resistance qualities are all included in his analysis [54]. MMC reinforced with Al matrix particles up to 30 wt% with three different sizes and weight fractions using a vortex technique and then applying pressure, and studied the effect of Al₂O₃ particle size and content on the mechanical properties of the composites, including tensile strength and hardness. He said that when the particle size decreased and the particle weight fraction increased, the hardness and tensile strength of the composites also improved [55].

In the study conducted by Adib and Abedinzadeh, AMCs reinforced with different proportions of SiC/Al₂O₃ nanoparticles of 5, 7.5, 10 wt. % were produced using powder metallurgy. The samples were produced by conventional milling and hot pressing methods. The distribution of nanoparticles for homogeneous in the aluminum matrix was verified by microstructural analysis. They claimed that the wear mechanism was abrasive wear combined with oxidative wear and demonstrated that the hardness and wear resistance of the nanocomposite samples increased with a 10% weight increase in the reinforcing content. [56]. Al6082 matrix and B₄C reinforced MMCs by powder metallurgy technique. The reinforcement weight ratios were selected as 0, 3, 6 and 9%, and the powders were mixed by cold/ball milling and compaction. Then, the temperature was kept at 1200 °C in a tubular furnace for sintering. They performed pressure, hardness and impact tests on the magnesium boron carbide composite samples they produced. As a result of their research, they found that increasing B₄C by 9% weight provided superior mechanical properties. They said that unreinforced magnesium alloys have lower mechanical properties compared to boron reinforced magnesium composites and that the good blend between B₄C

and Mg alloy creates intermetallic bonds efficiently and provides homogeneous distribution [57]. Wear behavior of Al6061-T6 discretely reinforced with silicon carbide and aluminum oxide composite. The tests were performed according to ASTM standards and used a pin-on-disc tester. Empirical relationships were established to predict wear results using statistical regression analysis and analysis of variance (ANOVA). It was shown that the wear resistance of 15% hybrid composite was higher than that of 5% composite [58].

Large diameter silicon carbide monofilament is used to reinforce a traditional titanium alloy matrix in the titanium metal matrix composites being researched for application in aeroengines. Composites made of titanium metal matrix (TMC) provide greater strength and stiffness along with the resulting potential for weight reduction. Weight reduction in rotors has been the focus of component studies and test parts produced in recent years. This offers the surrounding static structural components the chance to lose even more weight. Composites made of titanium metal matrix are becoming a popular choice for high-performance, nimble aircraft of the future. Ti matrix composite materials provide high specific strength, strength/lightweight, and hardness compared to Cu, Ni, and other iron-based materials. TMCs can provide a major advantage, such as greater weight reduction over other alloys, while maintaining equivalent strength and stiffness in high-temperature operating environments. The special and unique properties of TMCs have made them popular materials for extensive research and development programs in use. Considering the studies and areas of use of TMC material systems, they are the subject of significant advances in research. [59-65].

Produced Ti-6Al-4V alloy nano SiC reinforced MMCs at different ratios of 0, 5, 10 and 15%. They investigated the effects of adding nano SiC particles on the mechanical properties such as hardness and compressive strength of MMCs [66-68]. General microstructural properties and mechanical properties of Ti-TiBw composites with various matrix compositions and TiBw volume fractions based on their previous research and other studies. They also discussed the future development directions of Ti matrix alloys in terms of microstructure control and mechanical properties and the realistic possibilities of near-term commercial applications in industry [69]. TMCs have many different properties, including high temperature working properties, good wear resistance, and good corrosion resistance, and are preferred due to these properties. They stated that SiC, Al₂O₃, Si₃N₄, TiN, TiC, TiB and TiB₂ compounds are commonly used reinforcements. In their study, they used the investment casting process, which is easier and cheaper. A pin-on-disc wear tester was used to examine the wear and friction behavior of TMCs under several circumstances. The results were evaluated using scanning electron microscope (SEM) analysis [70]. Tensile behavior and

microstructure of TMCs reinforced with Ti and B4C using an in-situ reaction (TiB+TiC). They found that the tensile strength and ductility of B4C-doped alloys increased and decreased as the TiC and TiB contents increased, compared to the unreinforced pure Ti. They also stated that TMCs produced using 150 μm B4C exhibited slightly improved strength and showed a large tensile elongation of 61-117% compared to 1,500 μm B4C [71].

Considering the criteria such as the development of superior materials, cheapness, lightness, toughness, strength and environmental impact, MMCs are gaining more and more importance every day, but the inadequacy of traditional materials in meeting these needs makes the production and development of composite materials inevitable. Especially since motor vehicle manufacturers have set their goals to reduce fuel consumption and carbon emissions, the use of composite materials in vehicles has become more important than traditional materials due to their high strength/lightness ratio [72,73]. Reinforced magnesium matrix (AZ91) composite materials were produced using the stir casting method at 7500C. He also emphasized that the wetting problem between B4C and liquid Mg should be eliminated in order to obtain high properties. As a result of the microstructural examination performed with high resolution FEG-SEM, it was determined that the thin layer formed at the interface consists of Mn-C and Al-B compounds [74]. Wear behavior of Mg-based SiC reinforced composites. Wear tests were performed using 10 and 30N loads and a sliding speed range of 0.2–5.0 m/s using a pin-on-disc configuration against a hardened tool steel counter surface. While good results were obtained at low loads, they reported that wear resistance was not as definite at high loads. Post-wear SEM examinations yielded results such as oxidation, delamination, adhesion, thermal softening, and melting [75-78]. SiC particle reinforced AZ91D Mg composite and dispersed it in molten metal with the help of ultrasonic nonlinear effect. Despite the presence of a few tiny agglomerates (less than 300 nm), experimental results indicate that SiC nanoparticles are nearly evenly distributed and well dispersed in the magnesium matrix. Additionally covered is the relationship between nanoparticles and ultrasonic waves. The ability of ultrasonic manufacturing to quickly create a variety of metal matrix composites enhanced with nanoparticles is impressive [79].

6. GENERAL RESULTS

This research is related to light alloys and composites. It is about tensile strength, density, hardness, impact, corrosion, compression and porosity as well as friction (wear) properties of Al, Ti and Mg alloys produced by PM technique.

The significance of magnesium alloy, its mechanical and physical characteristics, and its uses in aerospace, transportation, and automobiles are illustrated in this review study. Magnesium alloys often have low density, excellent strength, and minimal corrosion.

In the increasing search for special materials, the most suitable lightweight materials that can be used instead of heavy metals (steel and cast iron) will be Al, Mg and Ti) alloys. Mg and its alloys are currently limited in their use in aircraft and space vehicles, but with the development of new production methods, it has been shown that these materials can also be used.

Metal matrix composites have higher mechanical properties than alloys. The basis of the high properties of composites is that defects such as porosity reduction and poor wetting can be reduced with the help of powder metallurgy. Providing reinforcement dimensions and homogeneous distributions with the powder metallurgy method provides better results compared to other methods, as well as increasing good strength and hardness. As a result, the production and use of MMCs with powder metallurgy techniques is gaining an important place in many sectors.

REFERENCES

1. Sarıtaş, S., (1995). Engineering metallurgy and materials, Ankara, Türkiye, 5–30.
2. Kalemtaş, A., (2014). Metal matrisli kompozitlere genel bir bakış, *Putech&Composites*, 22 ,18-30.
3. Kumar, A., Rai., R. N., (2018) Fabrication, Microstructure and Mechanical Properties of Boron Carbide (B4Cp) Reinforced Aluminum Metal Matrix Composite-A Review, *Materials Science and Engineering*, **377** 012092
4. Mortensen, A., “Metal matrix composite in industry: An Overview” http://mmc-assess.tuwien.ac.at/public/mmc_in_ind.pdf.
5. <https://www.slideshare.net/slideshow/aluminium-and-its-alloy/178071095>
6. Varol T., (2012). AA2024 Matrisli B4C Parçacık Takviyeli Metal Matrisli Kompozitlerin Toz Metalurjisi Yöntemiyle Üretimi Ve Özelliklerinin İncelenmesi, Yüksek Lisans Tezi, *Karadeniz Teknik Üniversitesi Fen Bilimleri Enstitüsü*, Trabzon.
7. Cihad, N., (2013). Alüminyum Matrisli B4c Parçacık Takviyeli Kompozitlerin Toz Metalurjisi Yöntemiyle Üretimi Ve Mekanik Özelliklerinin İncelenmesi, Yüksek Lisans Tezi, *Konya Selçuk Üniversitesi*, Konya.
8. Mordike B.L., Ebert T., (2001). Magnesium Properties, Applications and Potential, *Mat. Sci. Eng. A*, 302, 37-45.
9. Akkaş, M., & Gürdal, M. (2025). Effect on Machinability Characteristics of Cryogenic Process and Performance Assessment by Using Machine Learning Approach with Scaled Conjugate Gradient Algorithm. *Iranian Journal of Science and Technology, Transactions of Mechanical Engineering*, 1-20.
10. Benedyk J.J., (2004). Magnesium Challenges Aluminum Dominance as the Light Metal of Choice in Automotive Markets, *Light Metal Age-The International Magazine of Light Metal Industry*, October.
11. American Society for Testing and Materials-ASM, *Metal Handbook, Forming and Forging*, 14, p: 791-804, 9th Edition, 1988.
12. Kaya A. A., Özdoğru E.F., Abanoz D., Yiğit S., Yücel O., (2002). Otomotivde Magnezyum Alaşım Uygulamaları, OTEKON’02, *Otomotiv Teknolojileri Kongresi*, Bursa, 24-26.
13. Duygulu Ö., Oktay G., Kaya A.A., (2006). The Use of Magnesium Alloys in Automotive Industry, OTEKON’06, *Otomotiv Teknolojileri Kongresi*, Bursa, 26-28.

14. Kaya A.A., Pekgülyüz M., Türkoğlu S., (2004). Özdoğru E.F., Ağrılık Tasarrufu Amacıyla Otomobil Motor Bölmesinde Magnezyum Alaşımlarının Kullanımı, OTEKON'04, *Otomotiv Teknolojileri Kongresi*, Bursa.
15. Akkaş, M. (2024). The effect of molten salt on the mechanical properties and microstructure of CuNiSi alloys with reinforced Fe. *Science of Sintering*, (00), 28-28.
16. Fredrich H., S. Schumann, (2001). Research for a New Age of Magnesium in the Automotive Industry, *J. Mat. Proc. Tech.*, 117, 276-28.
17. Furuya H., Kogiso N., Matunaga S., Senda K.,(2001). Applications of Magnesium Alloys for Aerospace Structure Systems, *Materials Science Forum*, 341-348, 350-351.
18. Froes F.H., Eliezer, D., Aghion, E., (1998).The Science, Technology, and Applications of Magnesium. *J. Mat. Proc. Tech.*, 50 (9), 30-34.
19. Chaffin G.N., J.E. Jacoby, (1998).Guidelines for Aluminum Sow Casting and Charging, *The Aluminum Association*, Washington, D.C.
20. Rudd A.L., Breslina C.B., Mansfeld F. , (2000). The Corrosion Protection Afforded by Rare Earth Conversion Coatings Applied to Magnesium, *Corros. Sci.*, 42, 275-288.
21. Akkaş, M., K TABONAH, T. M., A ELFGHI, A. M., & Özorak, C. (2023). POWDER METALLURGICAL FABRICATION OF CO REINFORCED CUNISI MATRIX COMPOSITES: MICROSTRUCTURAL AND CORROSION CHARACTERIZATION. *Technological Applied Sciences*, 18(4), 64-74.
22. Wang Y., Wang Q., Ma C., Ding W., Zhu, Y., (2003). Effects of Zn and Re Additions on the Solidification Behavior of Mg-9Al Magnesium Alloy, *Mater. Sci. and Eng. A*, 342, 178-182.
23. Tegenkamp C., Michailov M., Wollschlager J., Pfnur H., (1999). Growth and Surface Alloy Formation of Mg on Ag 100, *Appl. Surf. Sci.*, 151, 40-48.
24. Watanabe H., Tsutsui H., Mukai T., Kohzu M., Tnabe S., Higashi K., (20019). Deformation Mechanism in a CoarseGrained Mg-Al-Zn Alloy at Elevated Temperatures, *Int. J. Plasticity*, 17, 387-397.
25. Kaneko J., Sugamata M., Numa M., Nishikawa Y., Takada H., (2000). Effect of Texture on the Mechanical Properties and Formability of Magnesium Wrought Materials, *J. Jpn. I. Met.*, 64 (2),141-147.
26. Özorak, C., Tabonah, T. M. K., & Akkaş, M. (2023). Production of CuNiSi Composites by Powder Metallurgy Method: Effects of Ti on the

- microstructural and corrosion properties. *European Journal of Technique (EJT)*, 13(2), 88-93.
27. Mwembela A., Konopleva E.B., McQueen H.J., (1997). Microstructural Development in Mg alloy AZ31 During Hot Working, *Scripta. Mater.*, 37 (11), 1789-1795.
 28. Akkaş, M. (2022). Synthesis and characterization of MoSi₂ particle reinforced AlCuMg composites by molten salt shielded method. *Türk Doğa ve Fen Dergisi*, 11(4), 11-17.
 29. Takuda H., Fujimoto H., Hatta N., (1998). Modelling on Flow Stress of Mg–Al–Zn Alloys at Elevated Temperatures, *J. Mat. Proc. Tech.*, 80-81, 513-516.
 30. Keeler S.P., Backofen W.A., (1963). Plastic Instability and Fracture in Sheets Stretched over Rigid Punches, *Transactions of the American Society for Metals*, 56, 25-48.
 31. Doege E., Sebastian W., Droder K., Kurtz G., (2001). Increased Formability of Mg-Sheets Using Temperature Controlled Deep Drawing Tools, in: M.Y. Demeri (Ed.), (20019. Innovations in Processing and Manufacturing of Sheet Materials, *The Minerals, Metals and Materials Society*, 53-60.
 32. Ghosh S., Kikuchi N., (1988). Finite Element Formulation for Simulation of Hot Sheet Metal Forming Process, *Int. J. Eng. Sci.* 26 (2), 143-161.
 33. Bolt P.J., Werkhoven R.J., Van de Boogaard A.H., (2001). Effect of Elevated Temperature on the Drawability of Aluminum Sheet Components, in: *Proceedings of the ESAFORM*, 769-772.
 34. Jayasathyakawin, S., Ravichandran, M., Baskar, N., Anand Chairman, C., Balasundaram, R., (2020). Mechanical properties and applications of Magnesium alloy – Review, *Materials Today: Proceedings*, 27(2), 909-913.
 35. Akkaş, M., & Elfghi, A. M. A. (2022). TiB₂ parçacık takviyeli alcumg kompozitlerin üretilebilirliğinin araştırılması. *Uluslararası Doğu Anadolu Fen Mühendislik ve Tasarım Dergisi*, 4(2), 118-128.
 36. Avedesian, M., Baker. H., (1999). Magnesium and Magnesium Alloys. Eds: M ASM Speciality Handbook, *The Materials Information Society*, ASM International.
 37. Demir Dışı Metallerin Kaynağı, Burhan Oğuz, *Oerlikon Yayını*, 1990
 38. P. Alan A. Luo, (2021). “Magnesium Overview&Applications”, *Magnesium Training 101, 78th Annual Magnesium Conference*, International Magnesium Association.

39. Caligulu, U., Durmus, H., Akkas, M., & Sahin, B. (2021). Microstructure and mechanical properties of Ni matrix B₄C reinforced functionally graded composites. *Science of Sintering*, 53(4), 475-484.
40. Ducker Research&Consulting, (2021). “Automotive Materials in an Electrified World, Understanding the Role of Materials in Meeting CO₂ Requirements”, *78th Annual Magnesium Conference*, International Magnesium Association.
41. Fabrizio D’Errico, (2021). “Advancements in Low-Flammable Mg-CaO Alloy Systems Processed by Two Environmentally Friend Processes: Hot Extrusion of No-Remelt Recycling Chips and Inert Gas Assisted High Pressure Die Casting”, *78th Annual Magnesium Conference*, International Magnesium Association.
42. Daisuke Konishi, Kazumasa Yamazaki, (2021). “Activities of Japan Magnesium Association and Progress of Applications in Japan”, *78th Annual Magnesium Conference*, International Magnesium Association.
43. Akkaş, M., & Al, S. F. R. A. (2021). Effect of hot pressing and reinforcement of TiC and WC on the mechanical properties and microstructure of AlCuFeCrNi HEAs alloy. *Science of Sintering*, 53(1), 19-35.
44. European Aluminium Association, “Call on EU policymakers to address imminent supply shortage of Chinese magnesium”, *Position paper*, 27 September 2021
45. European Commission, *Critical Raw Materials for Strategic Technologies and Sectors in the EU*, A foresight Study, 2020
46. Dr. Jian Binfan, Prof. Xia Dehong, “Systematic Energy Saving and Low Carbon Technologies for Pidgeon Process Improvement”, *78th Annual Magnesium Conference*, International Magnesium Association, August 2021
47. ALCOA, (2015). “An Aluminum Company’s Perspective On Magnesium” *Come along for the ride*, IMA Vancouver, BC.
48. Akkaş, M. (2021). Production and characterization of boron carbide and silicon carbide reinforced copper-nickel composites by powder metallurgy method. *Materialwissenschaft und Werkstofftechnik*, 52(1), 32-42.
49. Merve Demirtaş, Ahmet Turan, Erman Car, Onuralp Yücel, (2017). “Kritik Hammaddeler”, *Metalurji ve Malzeme Mühendisleri Odası Metalurji Dergisi*, Sayı 183.
50. Tuğçe Ergül, Ahmet Turan, Erman Car, Onuralp Yücel, (2019)“Magnesium in Aluminium Alloys as an Alloying Element”, ALUS09.

51. Brian Cantor, Fionn Dunne and Ian Stone, 'Metal and Ceramic Matrix Composites, Institute of Physics Publishing, *Bristol and Philadelphia* 2004.
52. Ezugwu, E.O. and Wang, Z.M., August (1997). Titanium Alloys and Their Machinability, *Journal of Materials Processing Technology*, 262.
53. Fantel, R.J., Buckingham, D.A., Sullivan, D.E., (1986). Titanium Minerals Availability Market Economy Countries, United States Department of the Interior Bureau of Mines, *US Government Printing Office, Washington DC*.
54. Okabe, T.H. and Waseda, Y., June (1997). Producing Titanium through an Electronically Mediated Reaction, *Journal of the Minerals Metals & Materials Society*, 28.
55. Sherman, A.M., Sommer, C.J. and Froes, F.H., (1997). The Use of Titanium in Production Automobiles: Potential and Challenges, *Journal of the Minerals Metals & Materials Society*, 38.
56. Ozkaya, S A. Canakci (2016). Effect of the B4C content and the milling time on the synthesis, consolidation and mechanical properties of AlCuMg-B4C Nano composites synthesized by mechanical milling. *Powder Technology* 297, 8-16.
57. Dandan G., Xinbo H. , Zhang, R., Qu, X., (2017) Microstructure and tensile properties of in situ polymer derived particles reinforced steel matrix composites produced by powder metallurgy method. *Materials Science & Engineering A* 705, 231-238.
58. Akkaş, M. (2020). The mechanical and corrosion properties of WCCo–Al coatings formed on AA2024 using the HVOF method. *Materials Research Express*, 7(7), 076515.
59. Sung-Mo Hong, Jin-Ju Park, Eun-Kwang Park, Kyeong-Youl Kim, Jung-Gu Lee, Min-Ku Lee, Chang-Kyu Rhee, Jin Kyu Lee. Fabrication of titanium carbide Nano-powders by a very high speed planetary ball milling with a help of process control agents. *Powder Technology* 274 (2015) 393, 401.
60. M. Cabezaa, I. Feijoo, P. Merino, M.C. Pérez, S. Cruz, P. Rey. Effect of high energy ball milling on the morphology, microstructure and properties of Nano-sized TiC particle-reinforced 6005A aluminium alloy matrix composite. *Powder Technology* 321 (2017), 31-43.
61. Seonghyeon Na, Donghyun Yoon, Jaehoon Kim Hongkyu Kim, Donghoon Kim. An evaluation of the fatigue crack propagation rate for powder metallurgical nickel-based super alloys using the DCPD method at elevated temperatures. *International Journal of Fatigue* 101 (2017) 27 35.

62. Abhijit Dey, K. M. Pandey, and S. R. Maity, Fabrication of metal matrix composites by powder metallurgy: A review Guttikonda Manohar, *Conference Paper in AIP Conference Proceedings* · April 2018.
63. Gök, D. A., Bayraktar, C., Hoşkun, M., (2024). A review on processing, mechanical and wear properties of Al matrix composites reinforced with Al₂O₃, SiC, B₄C and MgO by powder metallurgy method, *Journal of Materials Research and Technology*, Volume 31, Pages 1132-1150,
64. Singh H. (2023). A critical review of mechanical and wear resistance characterizations on developed aluminium matrix composite reinforced with MgO particulates. *Journal of Computers, Mechanical and Management*, 2(4):23088–100.
65. Kok, M., (2005). Production and mechanical properties of Al₂O₃ particle-reinforced 2024 aluminium alloy composites, *Journal of Materials Processing Technology*, Volume 161, Issue 3, Pages 381-387,
66. Adib MH, Abedinzadeh R. (2023). Study of mechanical properties and wear behavior of hybrid Al/(Al₂O₃+SiC) nanocomposites fabricated by powder technology. *Materials Chemistry and Physics*, 305:127922–31
67. Gummadi AK, Gupta MK, Raviteja D, Babu AM, Niranjan RS, Patel PB. (2023). Investigations on mechanical behavior of processed MMCs of Al6082 and reinforcement particles B₄C by powder metallurgy technique, *Materials-today-proceedings*, 77:534–9.
68. Umanath K., Palanikumar K, Selvamani ST., (2013). Analysis of dry sliding wear behaviour of Al6061/SiC/Al₂O₃ hybrid metal matrix composites. *Composites Part B: Engineering*, 53:159–68.
69. Muhammad D. Hayat, Harshpreet Singh, Zhen He, Peng Cao, (2019). Titanium metal matrix composites: An overview, *Composites Part A: Applied Science and Manufacturing*, Volume 121, Pages 418-438,
70. Sivakumar, G., Ananthi, V., Ramanathan, S., (2017). Production and mechanical properties of nano SiC particle reinforced Ti–6Al–4V matrix composite, *Transactions of Nonferrous Metals Society of China*, Volume 27, Issue 1, Pages 82-90.
71. Ravi Chandran KS, Panda KB, Sahay SS., (2004). TiB_w-reinforced Ti composites: processing, properties, application prospects, and research needs. *JOM* , 56(5):42–8
72. Kim IY, Choi BJ, Kim YJ, Lee YZ., (2011)., Friction and wear behavior of titanium matrix (TiB+TiC) composites. *Wear*, 271(9):1962–5.
73. Em Akra, K. M., Akkaş, M., Boz, M. U. S. T. A. F. A., & Seabra, E. (2020). The production of AZ31 alloys by gas atomization method and its characteristics. *Russian Journal of Non-Ferrous Metals*, 61, 332-345.

74. Choi B-J, Kim Y-J. (2013). In-Situ (TiB+TiC) particulate reinforced titanium matrix composites: effect of B4C size and content. *Metals and Materials International*, 19(6):1301–1307.
75. Tokaji, K., (2005). Effect of stress ratio on fatigue behaviour in SiC particulate-reinforced aluminium alloy composite, *Fatigue Fracture of Engineering materials structure*, 28, 539–545.
76. Lopez, V.H., Scoles, A., Kennedy, A.R., (2003), The thermal stability of TiC particles in an Al7wt.%Si alloy, *Materials Science and Engineering. A*, 356, 316-325.
77. Kerti, I., (2019). Microstructural Variations In Cast B4C-Reinforced Magnesium Matrix Composites, *International Journal of Engineering Research and Development*, 11(1), 18-24.
78. C.Y.H Lim, S.C Lim, M Gupta, (2003). Wear behaviour of SiCp-reinforced magnesium matrix composites, *Wear*, 255 (1-6), 629-637.
79. Jie Lan, Yong Yang, Xiaochun Li, (2004). Microstructure and microhardness of SiC nanoparticles reinforced magnesium composites fabricated by ultrasonic method, *Materials Science and Engineering: A*, 386(1–2), 284-290.

Chapter 3

SURFACE COATING TECHNIQUES

Adnan KESKİN¹, Musa KILIÇ²

¹ Materials and Manufacturing Engineering, Batman University,
243236011004@student.batman.edu.tr (ORCID: 0009-0008-1534-2886)

² Beşiri Organized Industrial Zone Vocational School, Batman University,
musa.kilic@batman.edu.tr, (ORCID:0000-0001-5808-6917)

1. INTRODUCTION

In many engineering applications, corrosion, wear, fracture and fatigue are problems that significantly affect the surface properties of materials. It has become very important to produce wear-resistant materials by strengthening the surface properties of metallic materials with composite coatings [1].

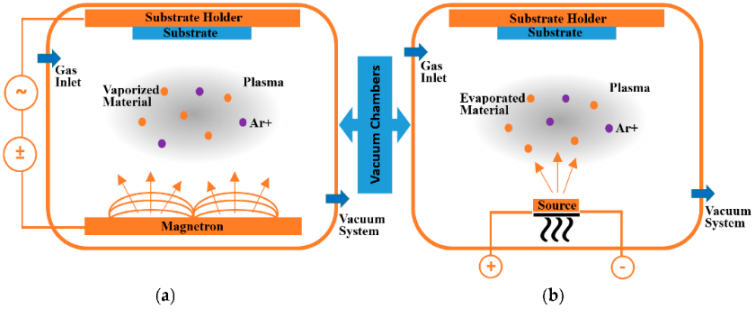
Coating methods are useful in specific applications where the desired functionality is paramount [2]. Each of these methods is suitable for different applications because they offer different deposition methods, different materials, second phases, and different thicknesses and densities [3]. Choosing the right materials for coating techniques is essential to a successful coating since they serve all protective functions. A protective layer can be made from a variety of materials, such as metals, ceramics, and polymers [4].

Surface coating techniques; hardfacing procedures like Gas Tungsten Arc Welding (GTAW), Plasma Transferred Arc Welding (PTA), and Laser Coating techniques; and thermal spraying techniques like Physical Vapor Deposition (PVD) Coating, Chemical Vapor Deposition Method (CVD), SOL-GEL, High Speed Oxy Fuel (HVOF), and Arc Wire Spray Coating will be covered.

2. THIN FILM COATINGS

2.1. Physical vapor deposition (PVD) Coating

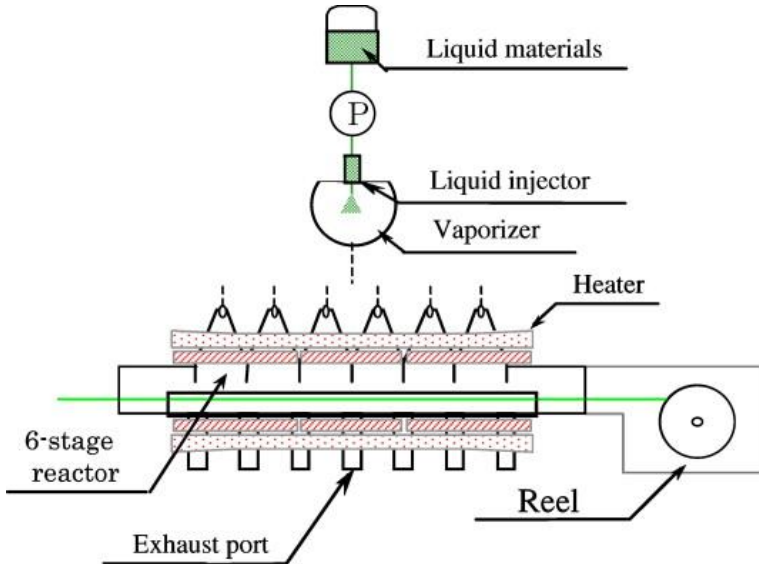
The coating formation process is largely based on physical evaporation. The thermal energy required for evaporation can be provided by various energy sources such as electron beam, heating wire, laser beam or molecular beam [5]. The physical vapor deposition process provides advantages such as corrosion and wear resistance and thin protective films on the surface of materials exposed to corrosive environments, and its application areas range from decorative objects to industrial parts [6]. It has widespread uses in metal forming, metal cutting (chipless), plastic injection molding, metal injection molding, mechanical components and abrasive applications [7].



Şekil 1.1. Schematic of PVD processes: sputtering (a) and evaporating (b) using Argon (Ar^+) gas [8].

2.2. Coating by chemical vapor deposition (CVD) method

On or close to a heated substrate surface, gaseous reactants undergo chemical reactions [9]. This coating is created by introducing the coating material as vapor at a specific temperature into a reaction chamber. The gas then either decomposes, reacts with, or is deposited onto a substrate in the reaction chamber [10]. With CVD, it is possible to produce almost any metallic or non-metallic element such as carbon and silicon, as well as carbides, nitrides, borides, oxides, intermetallics and many more compounds [11]. Additionally, CVD coating of polymers has shown itself to be a dependable method in a number of applications, including circuit boards, biomedical implants, and long-lasting lubricant coatings [12].



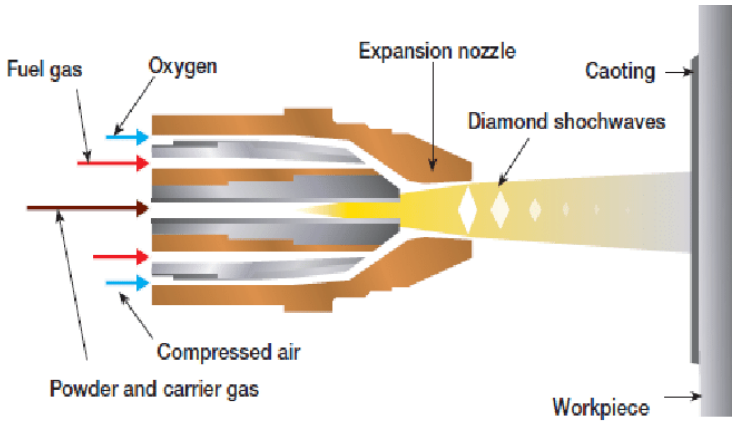
Şekil 1.2. Şematik kimyasal buhar biriktirme Şematik kimyasal buhar biriktirme (CVD) kurulumu, mekanik parçalar ve çalışma mekanizması [13].

3. THERMAL SPRAY COATINGS

Thermal spraying is a process that has a wide area of use in the industry for protecting surfaces against wear and corrosion [14]. Thermal spray coatings can be classified into different types according to their properties and process parameters.

3.1. High Speed Oxy-Fuel Coating (HVOF)

Figure 4 presents a schematic representation of the HVOF coating process. Fuel mixtures such as acetylene, propane, methane, hydrogen or natural gas are subjected to continuous combustion with oxygen in a combustion chamber to produce high-pressure hot gas vapor. This combustion chamber directs the combustion products to a nozzle to form a high-velocity spray; this velocity can exceed 1000 m/s [15]. The powdered coating ingredients are accelerated and injected into the hot jet stream after the combustion process, partially melting as they leave the nozzle tip. The semi-solid particles are guided to the substrate by this heated jet, creating a coating layer that can range in thickness from a few millimeters to several millimeters [16,17]. A multilayer coating produced using the HVOF method is depicted in Figure 3. Because of the coatings' strong adhesion, hardness, and low porosity and oxide, HVOF sprayed coatings have been employed extensively during the past ten years, primarily in the automotive, industrial, power plant, and aerospace industries [18].



Şekil 1.3. High velocity oxy-fuel (HVOF) coating system [19].

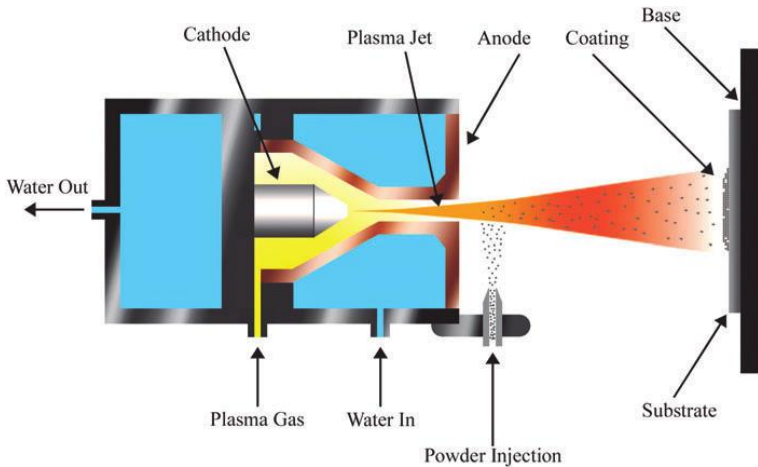
3.2. Plazma Sprey Kaplama

Plasma spraying is used to obtain wear-resistant coatings, thermal barrier coatings, etc. Plasma is formed by injecting gas into the arc chamber with high

temperature and high energy, which heats the raw material particles and accelerates them to hit the substrate. The plasma formed in the plasma gun accumulates by hitting the substrate in a molten form from the nozzle with high speed [20-23].

The liquid-based coating technique known as plasma spray has garnered a lot of interest because of its high deposition rate, production flexibility, intricate coating geometry, strong metallurgical bonding at the substrate-coating interface, and barriers that are resistant to wear, corrosion, and heat [24-26].

In addition to having excellent resistance to corrosion and wear, the resultant coating layer clings firmly to the substrate when exposed to high temperatures and surface tension [27,28]. Plasma spraying method is widely used in coatings of materials such as plastics, rubbers, metals and fibers [29].



Şekil 1.4. Plasma spray coating assembly and parts [30].

4. COATING WITH WELDING METHODS

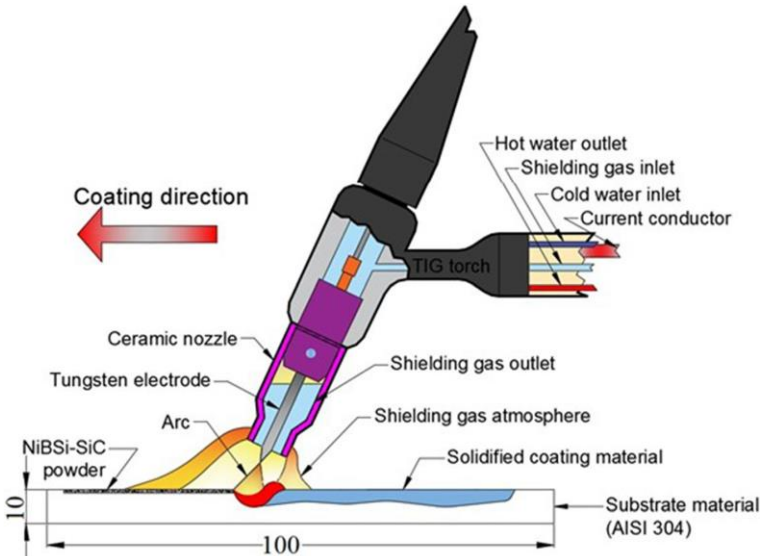
4.1. Coating with TIG Welding methods

In this method, the substrate surface and powder or hardfacing wire used for coating are melted using arc welding and then solidified, resulting in the formation of a new composite layer [31].

TIG welding method does not have a complex equipment like other methods, and it is a fast and easy method to obtain its equipment in the market. Other advantages of the method can be listed as low cost, high precision, energy and material savings. Coatings made using TIG welding method are more

economical, performance efficiency is better, the coatings formed are hard and also more resistant to wear [32,33].

In coating applications, cost effectiveness is also one of the important factors in the performance efficiency of the material after the process [34].



Şekil 1.5. Schematic picture of coating with TIG welding [35].

4.2. Plasma Arc Welding Coating

Welding coating methods are the coating of the worn surfaces of machine parts, especially those that wear under service conditions, by accumulating hard carbides and borides. Alloys with high carbon and chromium content are widely used in applications requiring wear resistance, such as mining, minerals, cement and paper industries [36].

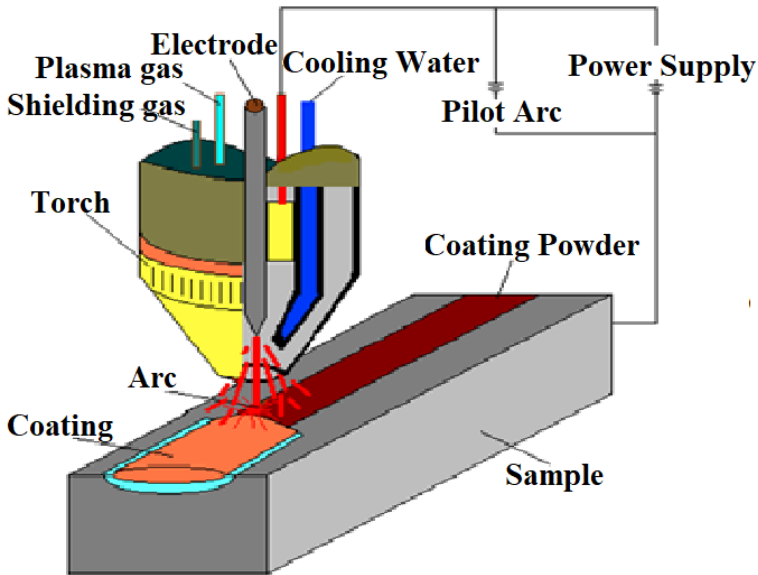
Plasma transfer arc welding process, one of these methods, is an efficient technology widely used in the manufacture of wear-resistant hard surfaces [37].

PTA technology has enabled the incorporation of hard carbide phases into metal matrix composites (MMCs) in industrial applications to produce high-quality coatings with good metallurgical bonding and low porosity, with high production efficiency and low cost [38, 39].

The method's basic idea is that the workpiece and powders that help produce hard phases like carbide and boride that are deposited on its surface, as well as the arc heat between the workpiece and a non-melting tungsten electrode, melt together to form a melt pool.

As the melt pool cools, the phases are created. The hard phases that occur can significantly enhance the material surfaces' performance [40-48].

Shipbuilding, electronics, nuclear, space, and aviation are just a few of the industries that have heavily utilized the PTA technique [49].



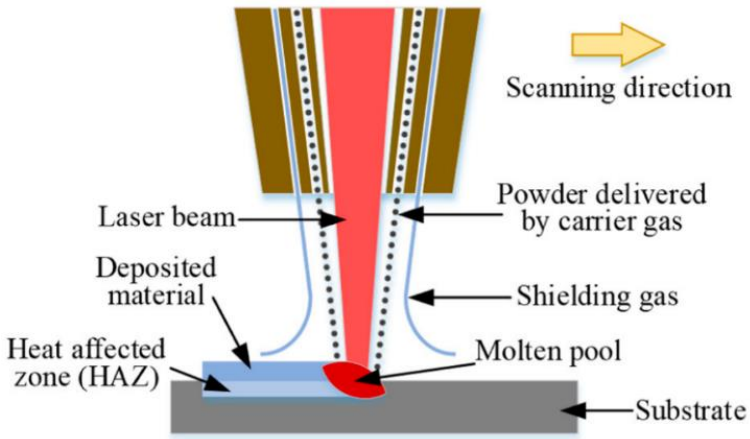
Şekil 1.6. Schematic picture of the coating process with PTA source [50].

4.3. Coating with Laser Welding Method

With the advent of additive manufacturing technology and the development of high-power lasers, the laser cladding process one of the best surface modification Technologies has grown in popularity [51, 52].

With a modest energy input, laser cladding produces a narrow heat affected zone (HAZ) and minimal microstructural distortion by coating various materials to form protective layers on the substrate's surface. [53, 54].

By utilizing the superior properties of the laser beam, hard, homogeneous, crack-free and non-porous layers with high wear and corrosion resistance can be obtained on metal surfaces [55, 56]. Laser coating method has been widely applied in the aviation, marine and petrochemical industries of machine equipment parts (crankshaft etc.) [57].



Şekil 1.7. Laser cladding schematic structure [58].

5. GENERAL RESULTS

There are several influencing parameters for successful coating deposition on a substrate, including deposition materials, substrate materials, raw material form (powder, wire, rods, precursors, etc.) and deposition methods. However, deposition processes are the most important, as they deal with the chemical change of materials in the coating layer and the alloying of the composition elements. Although these processes are reliable tools for material deposition and surface protection, they all have their drawbacks in different applications.

REFERENCES

1. Kılıç, M. (2021). Microstructural characterization of ni-Based B4c reinforced coMposite coating produced By tungsten inert gas Method. *Archives of Metallurgy and Materials*, 66(3), 917-924
2. Dehghanghadikolaei, A., Mohammadian, B., Namdari, N., & Fotovvati, B. (2018). Abrasive machining techniques for biomedical device applications. *J. Mater. Sci*, 5(1), 1-11.
3. Thakare, M. R., Wharton, J. A., Wood, R. J. K., & Menger, C. (2007). Exposure effects of alkaline drilling fluid on the microscale abrasion–corrosion of WC-based hardmetals. *Wear*, 263(1-6), 125-136.
4. DeMasi-Marcin, J. T., & Gupta, D. K. (1994). Protective coatings in the gas turbine engine. *Surface and Coatings Technology*, 68, 1-9.
5. de Damborenea, J. A. G. J., Navas, C., García, J. A., Arenas, M. A., & Conde, A. (2007). Corrosion–erosion of TiN-PVD coatings in collagen and cellulose meat casing. *Surface and Coatings Technology*, 201(12), 5751-5757.
6. Prengel, H. G., Pfouts, W. R., & Santhanam, A. T. (1998). State of the art in hard coatings for carbide cutting tools. *Surface and Coatings Technology*, 102(3), 183-190.
7. Baptista, A., Silva, F., Porteiro, J., Míguez, J., & Pinto, G. (2018). Sputtering physical vapour deposition (PVD) coatings: A critical review on process improvement and market trend demands. *Coatings*, 8(11), 402.
8. Van Stappen, M. B. A. W., Stals, L. M., Kerkhofs, M. B. A. W., & Quaeyhaegens, C. B. A. L. U. C. (1995). State of the art for the industrial use of ceramic PVD coatings. *Surface and Coatings Technology*, 74, 629-633.
9. Choy, K. L. (2003). Chemical vapour deposition of coatings. *Progress in materials science*, 48(2), 57-170.
10. Pahade, V. S., Chavan, P. S., & Baisane, V. P. (2016). A review paper on vapour deposition coating. *Int. J. Eng. Appl. Sci*, 3(6), 257640.
11. Doll, G. L., Mensah, B. A., Mohseni, H., & Scharf, T. W. (2010). Chemical vapor deposition and atomic layer deposition of coatings for mechanical applications. *Journal of thermal spray technology*, 19, 510-516.
12. Mori, M., Watanabe, T., Kashima, N., Nagaya, S., Muroga, T., Miyata, S., ... & Shiohara, Y. (2006). Development of long YBCO coated conductors by multiple-stage CVD. *Physica C: Superconductivity and its applications*, 445, 515-520.
13. Özel, S. (2013). Thermal Spraying Methods Used in Surface Coating Processes. *Bitlis Eren University Journal of Science*, 2(1), 88-97.

14. Thorpe, M. L., & Richter, H. J. (1992). A pragmatic analysis and comparison of HVOF processes. *Journal of Thermal Spray Technology*, 1, 161-170.
15. Fernández, J., Gaona, M., & Guilemany, J. M. (2007). Effect of heat treatments on HVOF hydroxyapatite coatings. *Journal of thermal spray technology*, 16, 220-228.
16. Scrivani, A., Bardi, U., Carrafiello, L., Lavacchi, A., Niccolai, F., & Rizzi, G. (2003). A comparative study of high velocity oxygen fuel, vacuum plasma spray, and axial plasma spray for the deposition of CoNiCrAlY bond coat alloy. *Journal of thermal spray technology*, 12, 504-507.
17. Akkaş, M. (2020). The mechanical and corrosion properties of WCCo–Al coatings formed on AA2024 using the HVOF method. *Material Research Express*. 7 (7), 076515, 1-18. DOI 10.1088/2053-1591/ab9fba.
18. Yadaw, R. C., Singh, S. K., Chattopadhyaya, S., Kumar, S., & Singh, R. C. (2018). Tribological behavior of thin film coating-a review. *Int. J. Eng. Technol*, 7(3), 1656-1663.
19. Karthikeyan, J., Berndt, C. C., Tikkanen, J., Reddy, S., & Herman, H. (1997). Plasma spray synthesis of nanomaterial powders and deposits. *Materials Science and Engineering: A*, 238(2), 275-286.
20. Parthasarathi, N. L., Duraiselvam, M., & Borah, U. (2012). Effect of plasma spraying parameter on wear resistance of NiCrBSiFe plasma coatings on austenitic stainless steel at elevated temperatures at various loads. *Materials & Design (1980-2015)*, 36, 141-151.
21. Mao, J., Ding, S., Li, Y., Li, S., Liu, F., Zeng, X., & Cheng, X. (2019). Preparation and investigation of MoSi₂/SiC coating with high infrared emissivity at high temperature. *Surface and Coatings Technology*, 358, 873-878.
22. Xiao, J. K., Wu, Y. Q., Zhang, W., Chen, J., Wei, X. L., & Zhang, C. (2019). Microstructure, wear and corrosion behaviors of plasma sprayed NiCrBSi-Zr coating. *Surface and Coatings Technology*, 360, 172-180.
23. Rezapoor, M., Razavi, M., Zakeri, M., Rahimipour, M. R., & Nikzad, L. (2018). Fabrication of functionally graded Fe-TiC wear resistant coating on CK45 steel substrate by plasma spray and evaluation of mechanical properties. *Ceramics International*, 44(18), 22378-22386.
24. Guo, H., Li, B., Lu, C., Zhou, Q., & Jia, J. (2019). Effect of WC–Co content on the microstructure and properties of NiCrBSi composite coatings fabricated by supersonic plasma spraying. *Journal of Alloys and Compounds*, 789, 966-975.

25. Huang, S., Sun, D., Wang, W., & Xu, H. (2015). Microstructures and properties of in-situ TiC particles reinforced Ni-based composite coatings prepared by plasma spray welding. *Ceramics International*, 41(9), 12202-12210.
26. Bulloch, J. H., & Callagy, A. G. (1999). An in situ wear-corrosion study on a series of protective coatings in large induced draft fans. *Wear*, 233, 284-292.
27. Knuutila, J., Ahmaniemi, S., & Mäntylä, T. (1999). Wet abrasion and slurry erosion resistance of thermally sprayed oxide coatings. *Wear*, 232(2), 207-212.
28. Nemani, S. K., Annavarapu, R. K., Mohammadian, B., Raiyan, A., Heil, J., Haque, M. A., ... & Sojoudi, H. (2018). Surface modification of polymers: methods and applications. *Advanced Materials Interfaces*, 5(24), 1801247.
29. Shin, K., Acri, T., Geary, S., & Salem, A. K. (2017). Biomimetic mineralization of biomaterials using simulated body fluids for bone tissue engineering and regenerative medicine. *Tissue Engineering Part A*, 23(19-20), 1169-1180.
30. Islak, S., Özorak, C., Sezgin, C. T., & Akkaş, M. (2016). Effect of boron on micro structure and microhardness properties of Mo-Si-B based coatings produced via TIG process. *Archives of Metallurgy and Materials*, 61.
31. Heidarshenas, B., Hussain, G., & Asmael, M. B. A. (2017). Development of a TiC/Cr₂₃C₆ composite coating on a 304 stainless steel substrate through a tungsten inert gas process. *Coatings*, 7(6), 80.
32. Fesharaki, M. N., Shoja-Razavi, R., Mansouri, H. A., & Jamali, H. (2019). Evaluation of the hot corrosion behavior of Inconel 625 coatings on the Inconel 738 substrate by laser and TIG cladding techniques. *Optics & Laser Technology*, 111, 744-753.
33. Liming Liu, Haifeng Xu, Jinkun Xiao, Xinlong Wei, Ga Zhang, Chao Zhang, Effect of heat treatment on structure and property evolutions of atmospheric plasma sprayed NiCrBSi coatings, *Surface & Coatings Technology* 325 (2017) 548–554, <http://dx.doi.org/10.1016/j.surfcoat.2017.07.011>.
34. Kilic, M., Imak, A., & Kirik, I. (2021). Surface modification of AISI 304 stainless steel with NiBSi-SiC composite by TIG method. *Journal of Materials Engineering and Performance*, 30(2), 1411-1419.

35. Gürgeç, T., & Özel, C. (2017). Effect of heat input on microstructure, friction and wear properties of Fe-Cr-BC coating on AISI 1020 surface coated by PTA method. *Turkish Journal of Science and Technology*, 12(2), 43-52.
36. Zikin, A., Antonov, M., Hussainova, I., Katona, L., & Gavrilović, A. (2013). High temperature wear of cermet particle reinforced NiCrBSi hardfacings. *Tribology International*, 68, 45-55.
37. Zhang, M., Li, M., Chi, J., Wang, S., Ren, L., Fang, M., & Zhou, C. (2019). Microstructure evolution, recrystallization and tribological behavior of TiC/WC composite ceramics coating. *Vacuum*, 166, 64-71.
38. Yung, D., Zikin, A., Hussainova, I., Danninger, H., Badisch, E., & Gavrilovic, A. (2017). Tribological performances of ZrC-Ni and TiC-Ni cermet reinforced PTA hardfacings at elevated temperatures. *Surface and Coatings Technology*, 309, 497-505.
39. Apay S., Gülenç B. (2013). Coating of Cobalt Base Powder onto Low Carbon Steel Surface Through PTA Method and Investigation of Coating Zone, *Duzce University Journal of Science and Technology* 1.1: 77-87.
40. Buytoz, S., Ulutan, M., & Yıldırım, M. M. (2005). Microstructural investigation of AISI 4340 steel hardfaced by TIG process. *Journal of Engineering and Architecture Faculty of Eskişehir Osmangazi University*, 18(1), 44-60.
41. Hou, Q. Y., J. S. Gao, F. Zhou (2005). Microstructure and wear characteristics of cobalt-based alloy deposited by plasma transferred arc weld surfacing. *Surface and Coatings Technology* 194.2: 238-243.
42. Bourithis, E., A. Tazedakis A., Papadimitriou G. (2002). A study on the surface treatment of “Calmax” tool steel by a plasma transferred arc (PTA) process. *Journal of Materials Processing Technology* 128.1: 169-177.
43. Deuis, R. L., J. M. Yellup J.M., C. Subramanian C. (1998). Metal-matrix composite coatings by PTA surfacing. *Composites science and technology* 58.2: 299-309.
44. Kucita P., Wang S.C., Li W.S., Cook R.B., Starink M.J. (2019). The effects of substrate dilution on the microstructure and wear resistance of PTA Cu-Al-Fe aluminium bronze coatings, *Wear* 440-441, 203102, <https://doi.org/10.1016/j.wear.2019.203102>
45. Deng X., Zhang G., Wang T., Ren S., Shi Y., Bai Z., Cao Q. (2019). Microstructure and oxidation resistance of a multiphase Mo-Si-B ceramic coating on Mo substrates deposited by a plasma transferred arc process, *Ceramics International* 45, 415-423, <https://doi.org/10.1016/j.ceramint.2018.09.182>

46. Dai W., Miao Y., Li J., Zheng Z., Zeng D., Huang Q. (2016). Investigation on morphology and micro-hardness characteristic of composite coatings reinforced by PTA copper alloying on nodular cast iron, *Journal of Alloys and Compounds* 689, 680-692, <http://dx.doi.org/10.1016/j.jallcom.2016.08.007>
47. Deng X., Zhang G., Wang T., Ren S., Li Z., Song P., Shi Y. (2019). Characterization and oxidation resistance of B-modified Mo₃Si coating on Mo substrate, *Journal of Alloys and Compounds* 807, 151693, <https://doi.org/10.1016/j.jallcom.2019.151693>].
48. Özel, S., Kurt, B., Somunkıran, İ. (2007). Plazma Transfer Ark Yöntemiyle FeCr/FeCr+ C tozunun düşük karbonlu çelik yüzeyine alaşımlanması. *Selcuk University Journal of Engineering Sciences*, 6(1), 21-30.
49. Yıldız T., Gür K.A. (2011). Effect of N₂ Gas on Coating Microstructure in FeMo Coating on AISI 1030 Steel Surface Produced by PTA Method " 6th *International Advanced Technologies Symposium (IATS'11)*, 16-18 May 2011, sayfa: 92-98, Elazığ, Turkey].
50. Muvvala, G., Karmakar, D. P., & Nath, A. K. (2017). Online assessment of TiC decomposition in laser cladding of metal matrix composite coating. *Materials & Design*, 121, 310-320.
51. Luo, X., Li, J., & Li, G. J. (2015). Effect of NiCrBSi content on microstructural evolution, cracking susceptibility and wear behaviors of laser cladding WC/Ni–NiCrBSi composite coatings. *Journal of Alloys and Compounds*, 626, 102-111.
52. Xu, P., Lin, C., Zhou, C., & Yi, X. (2014). Wear and corrosion resistance of laser cladding AISI 304 stainless steel/Al₂O₃ composite coatings. *Surface and Coatings Technology*, 238, 9-14.
53. Khalili, A., Goodarzi, M., Mojtahedi, M., & Torkamany, M. J. (2016). Solidification microstructure of in-situ laser-synthesized Fe-TiC hard coating. *Surface and Coatings Technology*, 307, 747-752.
54. Li, N., Xiong, Y., Xiong, H., Shi, G., Blackburn, J., Liu, W., & Qin, R. (2019). Microstructure, formation mechanism and property characterization of Ti+ SiC laser clad coatings on Ti6Al4V alloy. *Materials Characterization*, 148, 43-51.
55. Şimşek, T., Izciler, M., Ozcan, Ş., & Akkurt, A. (2019). Laser cladding of hot work tool steel (H13) with TiC nanoparticles. *Turkish Journal of Engineering*, 3(1), 25-31.9.

56. Lian, G., Zhang, H., Zhang, Y., Yao, M., Huang, X., & Chen, C. (2019). Computational and experimental investigation of micro-hardness and wear resistance of Ni-based alloy and TiC composite coating obtained by laser cladding. *Materials*, 12(5), 793.
57. Zhai, L., Ban, C., Zhang, J., & Yao, X. (2019). Characteristics of dilution and microstructure in laser cladding Ni-Cr-B-Si coating assisted by electromagnetic compound field. *Materials Letters*, 243, 195-198.
58. Wang, X., Lei, L., & Yu, H. (2021). A review on microstructural features and mechanical properties of wheels/rails clad by laser cladding. *Micromachines*, 12(2), 152.

Chapter 4

MORPHOLOGICAL AND TRIBOLOGICAL COMPARISON OF FE-BASED COATING AND Fe-WC COMPOSITE COATING IN LASER CLADDING METHOD

Fatih DEMİR¹, Mehmet EROĞLU², Necmettin IŞIK³

¹ Asst. Prof. Dr., Department of Machinery and Metal Technologies/Technical Sciences Vocational School, Batman University, Turkey, fatih.demir@batman.edu.tr, (ORCID: 0000-0003-3239-4641)

² Prof. Dr., Department of Metallurgy and Materials Engineering/Faculty of Engineering, Fırat University, Turkey, meroglu@firat.edu.tr, (ORCID: 0000-0002-5097-1943)

³ MSc, Department of Mechanical Engineering/ Institute of Graduate Studies, Batman University, Turkey, necmi7282@hotmail.com, (ORCID: 0009-0003-1901-7726)

INTRODUCTION

Surface engineering, as an engineering field based on the improvement of not only volumetric but also surface properties of materials, has gained increasing importance since the second half of the 20th century, and the surface coating techniques developed in this context have been the subject of in-depth research both academically and industrially. Laser cladding technology, which is one of the leading techniques developed to improve the surface properties of parts subjected to wear, corrosion and thermal load, stands out in modern engineering applications thanks to its high energy density, linear focusability, local process precision and the ability to establish a strong metallurgical bond between surface and substrate [1].

In most industrial laser systems, special gases (e.g. mixtures of carbon dioxide, helium, nitrogen, argon) of high purity and at constant pressures must be introduced into the laser tube to generate the laser beam. The choice and purity of the gases have a direct impact on the stability and processing efficiency of the laser beam. Thanks to their high processing speeds, precision and automation compatibility, laser systems have found wide use in strategic areas such as machine manufacturing, defense industry, space technologies and biomedical device production. In addition, the suitability of laser systems for mass production and low operating costs make this technology more attractive than traditional processing methods [2, 3].

One of the key factors determining the process quality in laser machining technologies is the selection of the correct and optimized process parameters. Parameters such as laser power, feed rate, focal spot position, powder or wire feed rate, scanning strategy, shielding gas flow rate, etc. directly affect the thermal effect fields resulting from the interaction of the laser with the workpiece and the microstructural integrity of the final product. Each parameter has an individual effect on the melting pool created by the laser, surface quality and thermomechanical deformations [3, 4]. Laser power, one of the most critical parameters, determines the total amount of energy transferred by the laser beam. As the laser power increases, the energy density transferred to the surface also increases, resulting in wider and deeper melt pools. However, high laser power used above a certain limit causes uncontrolled vaporization, microcrack formation and surface oxidation. Therefore, it is necessary to adjust the laser power in accordance with the targeted coating thickness, penetration depth and microstructural transformation [5, 6].

The feed rate determines the travel time of the laser beam on the workpiece and affects the total energy transferred to the surface. At low feed rates, the energy density increases due to the beam staying at one point for a longer time,

resulting in deeper penetration and thicker coating layers. However, very low feed rates can increase thermal damage; very high feed rates do not allow sufficient energy transfer and can cause insufficient melting and poor adhesion on the surface [7–9]. Powder feed rate is also an important variable affecting the coating quality. Insufficient powder feeding leads to insufficient material transfer to the melt pool created by the laser, while excessive powder feeding reduces the melting efficiency and can cause porosity and solidification defects on the surface. Therefore, the powder feed rate should be optimized together with the laser power and feed rate [3, 6]. Similarly, in layered manufacturing applications, even and controlled powder spreading plays a critical role in terms of the microstructure and surface roughness of the final product [7–9]. In addition, optical parameters such as focus position and laser spot diameter also affect the machining accuracy and surface character. The positioning of the focal spot relative to the workpiece surface directly determines the energy distribution profile, affecting the size and geometry of the heat affected zone (HAZ) that will occur during the process. Therefore, correct alignment and stabilization of laser optical systems is a prerequisite for a homogeneous and high-quality process [3, 4, 6].

Surface coating technology encompasses advanced engineering applications developed to improve the surface properties of materials, increase their functional life and provide resistance to environmental conditions. This technology serves a wide range of purposes, such as increasing surface hardness, improving wear and corrosion resistance, providing thermal insulation or modifying electrical/optical properties. Increasing the mechanical strength of material systems is not only achieved by volumetric modifications, but often by microstructural modification of the surface. Therefore, surface coating technologies are considered as an advanced application area of engineering beyond traditional bulk manufacturing processes [10, 11].

One of the most important factors in surface coating technologies is the bonding structure of the coating with the base material. Metallurgical bonding can be achieved especially in laser coating, plasma spray or diffusion coating techniques. This type of bond is formed by diffusion between the coating and the substrate at the atomic level under high temperature and short-term processing conditions, resulting in high adhesion strength. Researchers have reported that the bond structure formed on thermochemically treated steel surfaces offers more stable phase transitions and higher microhardness values than conventional coating methods [12, 13].

Surface coating technologies also enable the development of functional coatings. In this context, there are many special purpose applications such as

tribological coatings (providing resistance to wear and friction), thermal barrier coatings (providing insulation against heat) and biocompatible coatings (implant surfaces used inside the body). The powder or film materials used in these coatings can be metallic, ceramic or composite. Kumruoğlu et al. revealed that the surface structures obtained by electrolytic plasma method applied to medium carbon steel surfaces improve both tribological performance and hardness thanks to complex carbide phases [14].

The control of energy input in surface coating technologies is critical for process quality. High intensity energy sources such as laser, electron beam and plasma arc provide localized heating on the surface, making it possible to coat the desired areas. This not only increases energy efficiency, but also allows only the surface to achieve the desired properties without affecting the internal structure of the base material. Wang, et al. stated that tribo-oxides formed on laser-modified surfaces have positive effects on friction behavior and minimize material wear [15].

The future of surfacing technology is shaped by advanced engineering solutions such as smart coatings and multilayer structures. In this context, surface engineering has become not only a protection or strengthening technique, but also an integrated system design tool. Wang et al. emphasized that the electron beam treatments on AISI 4340 steel gave very successful results in terms of surface hardness and microstructural control in their surface modifications [16].

At the heart of this research is the consideration of the dynamic nature of the laser-powder-material ternary interaction as a key variable in determining properties such as coating homogeneity, phase transformations and tribological behavior. In the research, the effects of different powder material types and wear distance on laser cladding outputs are comparatively discussed.

1. EXPERIMENTAL STUDIES

In this study, the surface of commercially available St37 material was coated by laser cladding method using different powder mixtures. Firstly, 40x10x10 mm sized specimens were cut from St37 bars, which is the base material, and the surfaces of these specimens were ground and cleaned to make them engraved for coating. Coating powder consisting of a mixture of Fe (72 wt%) - FeCr (25 wt%) - FeMn (1 wt%) and FeSi (2 wt%) was used as matrix powder. In addition, a separate powder mixture was prepared by adding 40 wt% WC reinforcement powder to the aforementioned matrix powder. The prepared powder mixtures were first dried at 100 °C for 1 hour to eliminate the moisture content. Then the powder mixtures were mixed with sodium silicate to form a gel and applied as a layer on the surface of the base material (St37). The samples whose upper

surfaces were coated with coating powder in gel form were dried at 100 °C for 1 hour and made ready for the coating process.

The laser cladding process was performed at a scanning speed of 5 mm/s. Coating processes were completed in a laser welding device with a max. power capacity of 2 kW. Argon was used as shielding gas during the process (10 l/min). The produced samples and coating parameters are given in Table 1.

Table 1. Samples and cladding parameters

Sample No	Cladding material (Powder)	Scanning Speed (mm/s)	Laser Beam Power (W)
S1	No cladding	5	1400
S2	Fe based matrix	5	1400
S3	Fe based matrix with 40 wt% WC reinforcement	5	1400

After the coating process, samples were prepared from the coated materials for metallographic and tribological examinations. Sample cutting processes were completed in Presi Mecatome T260 cutting device. The metallographic samples were sanded and polished in Presi Minitech 233 manual polishing device and then etched in the etchant solution consisting of a mixture of HNO₃, HF, HCl and pure water. The coating surfaces of the wear specimens were ground and sanded to prepare them for the tests.

Scanning electron microscope (SEM) images were taken from the metallography specimens for microstructural investigations. Energy dispersive X-Ray (EDS) analysis was also performed. SEM and EDS analyses were performed on ThermoScientific Scios 2.

Abrasion tests were carried out on a Turkeyus ball-disc tribometer. The abrasion rates at 50m and 100m abrasion distances under 10N load were determined with the tests performed under dry and room temperature conditions. In addition, SEM images were taken from the worn surfaces with ThermoScientific Scios 2 device.

2. EXPERIMENTAL RESULTS AND EVALUATION

The SEM image of the S2 specimen without WC reinforcement shows the typical microstructure of the base material St37 and the cross-sectional morphology of the columnar coating composed of Fe-based matrix powder (Figure 1). For sample S2, it can be easily said that a successful connection between the coating layer and the base material has been formed.

During the initial phase of solidification, heat transfer from the molten coating pool to the substrate produces a strong cooling effect at the junction interface [17]. This results in the formation of a planar thin layer joining the base material and the coating. The high cooling rate near this layer leads to the formation of a columnar structure. Relatively rapid solidification in the direction of high heat transfer prevented the formation of grain boundaries perpendicular to the interface during the growth of columnar grains [18].

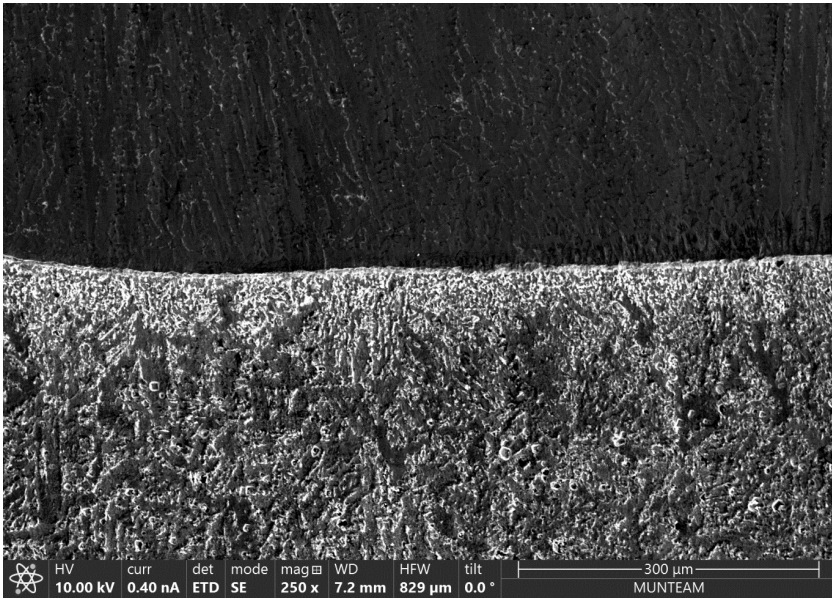


Figure 1. SEM image of sample S2

Figure 2 shows that the 40% WC reinforcement added to the matrix powder has no negative effect on the connection between the coating and the base material. In addition, the presence of a planar thin layer is observed at the interface of the S3 sample as in the S2 sample.

In the coating morphology of the S3 sample, unlike the S2 sample, solidification is also observed in the direction perpendicular to the columnar structure. The presence of unmelted WC particles in the coating pool caused the heat flow not only towards the base material but also towards these particles. This led to the formation of multidirectional micro-growths during solidification, resulting in a more refined localized microstructure [19].



Figure 2. SEM image of sample S3

When the EDS mapping scan of the S3 sample is examined, the elements that make up the matrix powder are distributed throughout the microstructure around the WC particles. Especially Fe and Mn elements were found to be slightly more concentrated at the WC boundaries.

When we consider the W and C elements, it is seen that most of the W element is found in WC particles and the rest of the W element is distributed throughout the coating microstructure. In the case of element C, there was a more balanced distribution. This distribution can be explained by the fact that element C takes a more active role in the formation of any possible carbide [18].

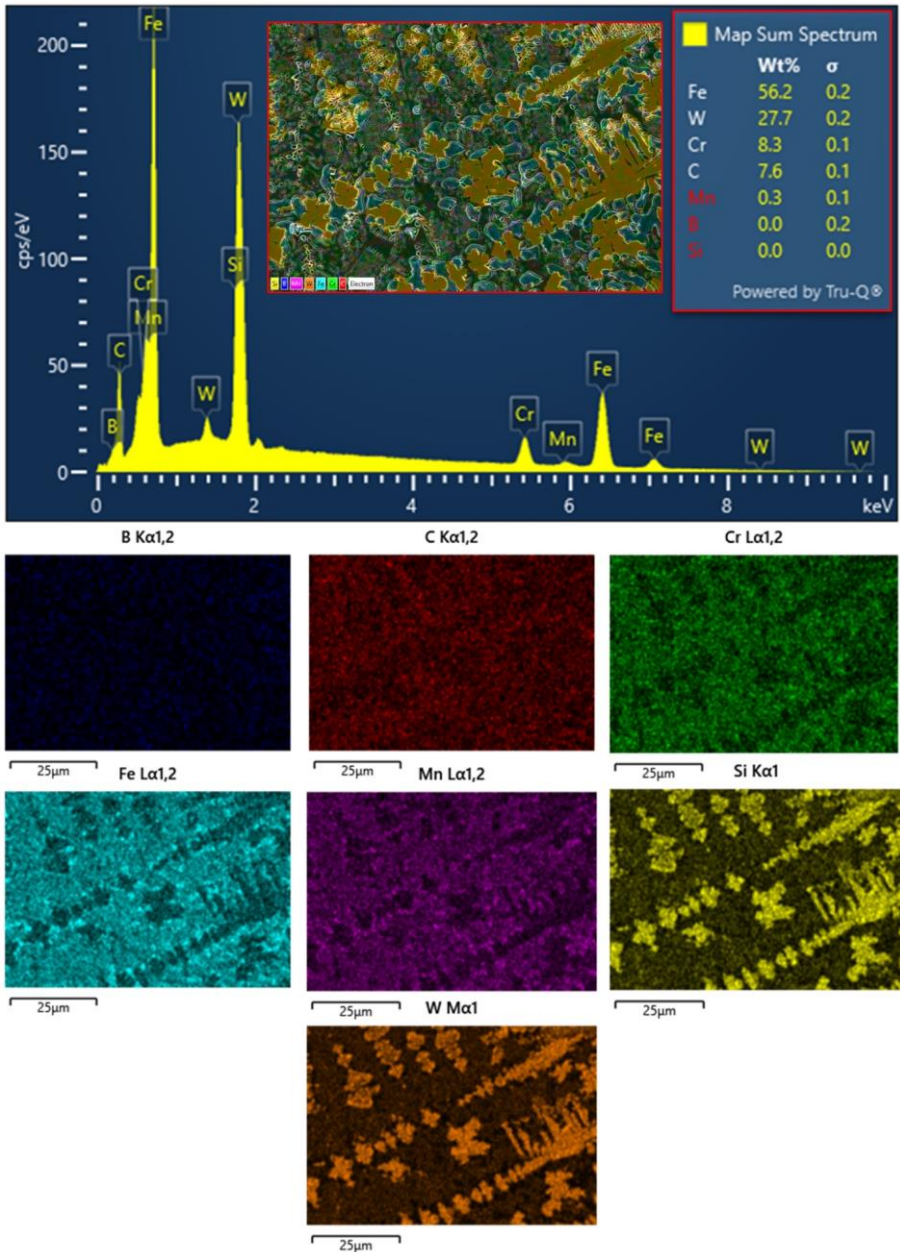


Figure 3. EDS analysis of sample S3

When we compare the wear rates of the coated specimens with St37 material, Fe-based coating material significantly improved the wear performance as expected (Table 2). WC reinforcement in the Fe-based coating matrix improved the wear resistance. This was the case for both 50m and 100m sliding distances.

Table 2. Wear rates of samples

Sample	Load (N)	Sliding distance (m)	Wear rate (mm ³)
S1		50	0.122
		100	0.170
S2	10	50	0.051
		100	0.079
S3		50	0.023
		100	0.032

When we examine the wear surface of St37 material, it is seen that the underlay material is severely worn with deep and continuous grooves, micro cracks and plastic deformation. Based on the SEM image, it can be said that abrasive wear is effectively realized for St37 material at a sliding distance of 50m (Figure 4).

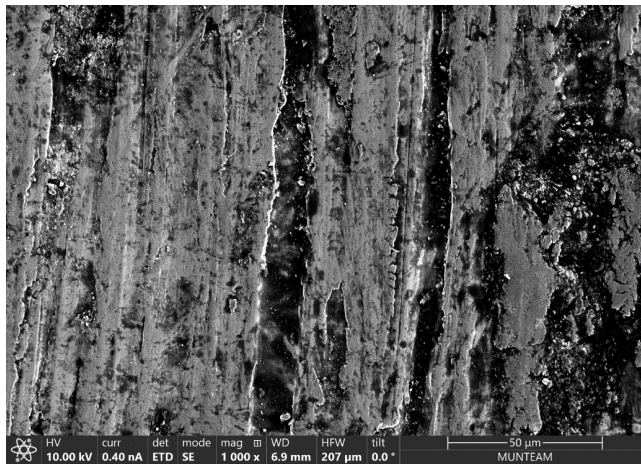


Figure 4. SEM image of the worn surface of sample S1

It is seen that tribo-surfaces are formed and debris is formed after 100m sliding distance in Fe matrix coating material (Figure 5). The wear surface image of specimen S2 shows that the wear mechanism for the Fe-based coating is adhesion wear and fatigue wear.

The wear surface image and wear rates of specimen S3 show that the wear resistance of WC reinforced WC-Fe composite coating is better than that of Fe based coating. This is because the addition of WC reinforcement increases the hardness of the coating [20]. In addition, the presence of WC in the coating prevents the entire surface from being in contact during wear and actually causes the contact area to be smaller. Therefore, the local stress at the contact points is

very large. This leads to excessive local stresses and sticking or welding of the contact points. As a result, it manifests itself as material peeling, which indicates that adhesion wear has occurred, as in Figure 6 [21].

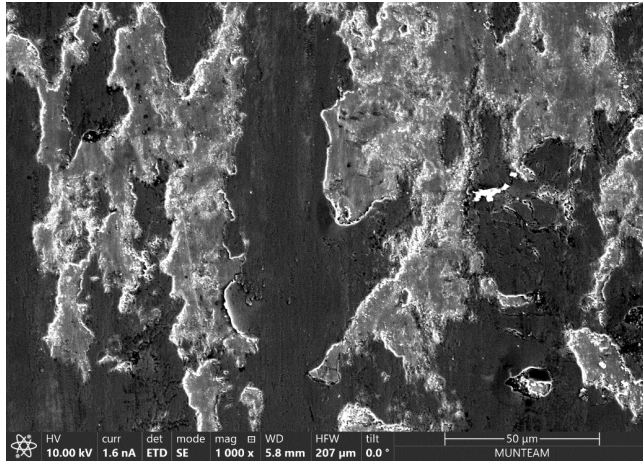


Figure 5. SEM image of the worn surface of sample S2



Figure 6. SEM image of the worn surface of sample S3

3. GENERAL RESULTS

In this study, WC-Fe composite coating and Fe-based coating materials were compared morphologically and tribologically as a result of the analysis and tests performed. The general results obtained are listed below.

- For Fe-based coatings, it was found that WC reinforcement does not cause joint problems and is suitable to be used as a reinforcing material.

- WC reinforcement produced multidirectional growth zones during solidification, resulting in a more refined microstructure.
- WC reinforcement improved the wear resistance by playing a decisive role on the effective wear mechanism.

ACKNOWLEDGMENTS

The laser welding device used for the surface coating applications was financed by Firat University Scientific Research Projects Unit (Project number: ADEP.23.15).

REFERENCES

1. Burakowski, T., & Wierzchon, T. (1998). *Surface engineering of metals: principles, equipment, technologies*. CRC press.
2. Artkin, F. (2022). Endüstriyel Lazer Teknolojilerinin Makine ve İmalat Alanındaki Uygulamaları. *ASES II. International Health, Engineering and Sciences Conference*, 38–44, Kayseri, Turkey.
3. Dindar, Ç., Altay, M., & Aydın, H. (2021). Lazer kaplama prosesi ve proses parametreleri: derleme çalışması. *Uludağ Üniversitesi Mühendislik Fakültesi Dergisi*, 26(2), 723-736.
4. Kattire, P., Paul, S., Singh, R., & Yan, W. (2015). Experimental characterization of laser cladding of CPM 9V on H13 tool steel for die repair applications. *Journal of Manufacturing Processes*, 20, 492-499.
5. Li, C., Sun, S., Zhang, Y., Liu, C., Deng, P., Zeng, M., ... & Wang, Y. (2019). Effects of laser processing parameters on microstructure and mechanical properties of additively manufactured AlSi10Mg alloys reinforced by TiC. *The International Journal of Advanced Manufacturing Technology*, 103, 3235-3246.
6. Cavaliere, P. (Ed.). (2021). *Laser Cladding of Metals*. Cham, Switzerland: Springer International Publishing.
7. Aydın, K., & Karamolla, M. (2019). Katmanlı İmalat ile Üretilen Metal Malzemelerin Kaynak Kabiliyeti. *Bitlis Eren Üniversitesi Fen Bilimleri Dergisi*, 8(4), 1610-1620.
8. Gabriel, T., Rommel, D., Scherm, F., Gorywoda, M., & Glatzel, U. (2017). Laser cladding of ultra-thin nickel-based superalloy sheets. *Materials*, 10(3), 279.
9. Sexton, L., Lavin, S., Byrne, G., & Kennedy, A. (2002). Laser cladding of aerospace materials. *Journal of Materials Processing Technology*, 122(1), 63-68.
10. Zhu, L., Xue, P., Lan, Q., Meng, G., Ren, Y., Yang, Z., ... & Liu, Z. (2021). Recent research and development status of laser cladding: A review. *Optics & Laser Technology*, 138, 106915.
11. Liu, H., Tan, C. K. I., Wei, Y., Lim, S. H., & Lee, C. J. (2020). Laser-cladding and interface evolutions of inconel 625 alloy on low alloy steel substrate upon heat and chemical treatments. *Surface and Coatings Technology*, 404, 126607.
12. Duradzhi, V. N., Lavrova, T. S., & Mokrova, A. M. (1986). Thermochemical treatment of steel in an electrolytic plasma. *Inorg. Mater.(Engl. Transl.);(United States)*, 21(9).

13. Cionea, C. (2010). *Microstructural evolution of surface layers during electrolytic plasma processing* (Doctoral dissertation, The University of Texas at Arlington).
14. Kumruoglu, L. C., Becerik, D. A., Ozel, A., & Mimaroglu, A. (2009). Surface modification of medium carbon steel by using electrolytic plasma thermocyclic treatment. *Materials and Manufacturing Processes*, 24(7-8), 781-785.
15. Wang, S. Q., Wei, M. X., & Zhao, Y. T. (2010). Effects of the tribo-oxide and matrix on dry sliding wear characteristics and mechanisms of a cast steel. *Wear*, 269(5-6), 424-434.
16. Wang, C. C., & Hwang, J. R. (1994). Surface hardening of AISI 4340 steel by electron beam treatment. *Surface and Coatings Technology*, 64(1), 29-33.
17. Shen, F., Tao, W., Li, L., Zhou, Y., Wang, W., & Wang, S. (2020). Effect of microstructure on the corrosion resistance of coatings by extreme high speed laser cladding. *Applied Surface Science*, 517, 146085.
18. Xiao, Q., lei Sun, W., xin Yang, K., feng Xing, X., hao Chen, Z., nan Zhou, H., & Lu, J. (2021). Wear mechanisms and micro-evaluation on WC particles investigation of WC-Fe composite coatings fabricated by laser cladding. *Surface and Coatings Technology*, 420, 127341.
19. Liu, X. M. (2006). Mechanism and control of the nickel based alloy+ WC laser cladded layer microstructure. *Applied Laser*, 5, 299-302.
20. Yang, L., Yu, T., Li, M., Zhao, Y., & Sun, J. (2018). Microstructure and wear resistance of in-situ synthesized Ti (C, N) ceramic reinforced Fe-based coating by laser cladding. *Ceramics International*, 44(18), 22538-22548.
21. Lei, J., Shi, C., Zhou, S., Gu, Z., & Zhang, L. C. (2018). Enhanced corrosion and wear resistance properties of carbon fiber reinforced Ni-based composite coating by laser cladding. *Surface and Coatings Technology*, 334, 274-285.

Chapter 5

DEVELOPMENT AND MICROSTRUCTURAL EVALUATION OF MECHANICALLY ALLOYED HIGH-ENTROPY ALLOYS SYNTHESIZED BY POWDER METALLURGY

Mehmet AKKAŞ¹

¹ Assoc. Prof. Dr., Department of Mechanical Engineering/Faculty of Engineering, Architecture and Design, Kahramanmaraş İstiklal University, Kahramanmaraş, Turkey, mehmet.akkas@istiklal.edu.tr, (ORCID: 0000-0002-0359-4743)

1. INTRODUCTION

In contemporary technological and industrial fields, applications that require sustained operation under elevated temperatures and dynamic mechanical loads have significantly driven the advancement of associated industries. These demanding working environments have necessitated the design and development of novel classes of materials, components, and structural systems capable of maintaining performance and reliability under such extreme conditions. In response to these challenges, a substantial body of research has been directed toward the formulation and optimization of innovative alloy systems that can demonstrate enhanced mechanical and thermal performance in harsh service conditions [1-5].

Within this framework, the concept of High-Entropy Alloys (HEAs), first introduced in 2004, represents a paradigmatic shift in alloy design methodology. Unlike conventional alloys, which are typically composed of one or two principal elements supplemented with minor additions for property enhancement, HEAs are characterized by the equiatomic or near-equiatomic incorporation of five or more principal elements. This multi-principal element design strategy contributes to unique thermodynamic and structural behaviors not observed in traditional alloy systems [6,7]. Due to their elevated configurational entropy, HEAs tend to stabilize into single-phase solid solutions with relatively simple crystal structures, even at high processing or service temperatures [8]. As the number of constituent elements increases, the formation of complex intermetallic or intermediate compounds—often associated with increased brittleness and localized stress concentration—is suppressed. Instead, these alloys preferentially form stable solid solution phases such as Body-Centered Cubic (BCC), Face-Centered Cubic (FCC), and Hexagonal Close-Packed (HCP) lattices [9]. These structural configurations are directly responsible for imparting superior mechanical attributes to the alloys, including but not limited to enhanced tensile strength, elevated hardness, wear resistance, corrosion resistance, thermal stability, oxidation resistance, creep resistance, and extended fatigue life [10-12].

Beyond their promising mechanical characteristics, HEAs have garnered considerable academic and industrial attention due to their refined and often homogenous microstructures, which contribute to reliable and reproducible material behavior. To further augment the performance of HEAs, especially in applications involving wear, high loads, or elevated temperatures, ceramic reinforcement phases such as Titanium Carbide (TiC) are often incorporated into the metallic matrix. This strategy significantly improves properties such as hardness, thermal stability, and melting point, enabling the design of metal matrix composites with multifunctional capabilities. For instance, in previous

investigations, TiC-reinforced aluminum-based HEAs exhibited a notable tensile strength of approximately 351.8 MPa along with an elongation to fracture of 5.6%, demonstrating their viability in structural applications requiring both strength and ductility. Moreover, WC-Co (Tungsten Carbide-Cobalt) systems, which are widely used in cutting tool industries, have shown potential to be substituted by TiC-based materials due to their comparable surface finishing quality, superior wear resistance, and high hardness. Notably, when used in conjunction with Titanium Diboride (TiB_2), TiC-based systems remain thermodynamically stable up to approximately 2600°C , underscoring their potential in high-temperature machining and forming operations. Furthermore, Tungsten Carbide (WC) itself offers excellent wear resistance, a high elastic modulus, and remarkable resistance to molten metal attack. The introduction of TiC particles into WC matrices further enhances their mechanical durability, particularly in terms of fracture toughness, plastic deformation resistance, and structural resilience [13-20].

Nevertheless, corrosion remains a critical failure mechanism for metallic systems, resulting in substantial economic losses. It is estimated that corrosion accounts for approximately 3% of global annual industrial output losses, underscoring its pervasive impact. While certain alloys naturally form passive oxide layers that provide some degree of protection against corrosive environments, such layers can be easily disrupted—especially under surface machining or drilling—leading to sudden degradation in material integrity and performance [26]. To counteract these effects, significant efforts are being directed toward the development of new alloy compositions that exhibit negative electrochemical potential and intrinsic corrosion resistance. However, studies specifically addressing the corrosion behavior of HEAs, particularly in ingot form, remain relatively limited in number. Available data suggest that the incorporation of aluminum—while beneficial for other properties—may negatively impact corrosion resistance due to the formation of an oxide layer on the alloy surface, especially in sulfuric acid environments at 27°C . Despite this, other investigations have demonstrated that the high entropy effect, which contributes to the homogeneous distribution of elements and structural stabilization, can play a beneficial role in mitigating corrosion, especially at elevated or evaporation temperatures [21-27]. Some HEAs have indeed shown satisfactory corrosion resistance under specific environmental conditions, indicating their suitability for use in corrosive service environments.

2. EXPERIMENTAL STUDIES

In this experimental study, metal powders of exceptionally high purity—each exhibiting an approximate compositional accuracy of 99.9%—and a standardized particle fineness of 325 mesh were selected as starting materials. The rationale behind utilizing powders of such precision was to facilitate the tunability of alloy properties, thereby enabling the deliberate modification and control of both mechanical and physical characteristics in accordance with experimental objectives and performance criteria. To achieve a homogeneous mixture at the microstructural level and promote effective alloying among the constituent elements, a mechanical alloying (MA) process was employed. This was conducted using a Retsch PM100 planetary ball mill operating at a rotational velocity of 425 revolutions per minute (rpm), sustained continuously for a milling duration of 12 hours. The planetary ball mill features a sealed powder containment vessel designed to isolate the powder blend from external contaminants, including oxygen and moisture, thus ensuring preservation of the elemental purity and minimizing any undesirable compositional deviations during processing. This protective containment mechanism is considered critical in achieving repeatable and high-integrity alloy synthesis.

Following the mechanical alloying stage, the uniformly mixed powders were subjected to a uniaxial compaction process using cold pressing methodology. The compaction was carried out under a constant applied pressure of 650 megapascals (MPa), utilizing a Specac GS15011 hydraulic press, which is housed in the Central Research Laboratory at Kastamonu University. The pressing operation was performed within a cylindrical die of 13 mm diameter, allowing for the fabrication of samples with consistent geometry and density distribution. This step not only provided the necessary structural form to the composite powders but also facilitated enhanced particle contact, setting the groundwork for successful sintering. Subsequent to compaction, the green samples underwent a sintering process inside an argon-atmosphere-controlled furnace, located in the Metallurgical and Materials Engineering laboratories of Kastamonu University. The sintering was conducted at a target temperature of 1215°C for a total soaking time of 240 minutes, following a precise heating schedule. The entire thermal cycle—comprising heating, soaking, and cooling—was designed to span 480 minutes in total. The heating rate was meticulously maintained at approximately 10°C per minute, ensuring gradual thermal exposure and the effective volatilization of residual processing contaminants, such as lubricants and adsorbed gases.

Once the samples reached the target sintering temperature, they were isothermally held at 1215°C for 4 hours to promote solid-state diffusion and metallurgical bonding across particle interfaces. This holding stage was of paramount importance, as it encouraged grain boundary development, phase homogenization, and densification within the powder matrix, ultimately contributing to the enhanced mechanical performance and structural cohesion of the sintered body. Following sintering, a controlled furnace-cooling procedure was applied to prevent the development of thermal stresses or cracking due to abrupt temperature gradients. The samples were cooled within the argon-filled furnace chamber at a carefully regulated rate until room temperature was reached. This slow and uniform cooling was essential for maintaining internal structural stability and avoiding microstructural defects.

After thermal processing, the sintered specimens were prepared for microstructural characterization using scanning electron microscopy (SEM). To this end, a series of standard metallographic procedures were systematically applied. Each sample was first embedded in bakelite resin under a temperature-controlled environment at approximately 120°C. This mounting process provided mechanical stability and ease of manipulation during subsequent surface preparation stages. The mounted specimens were then subjected to progressive grinding using silicon carbide abrasive papers of decreasing grit size, followed by precision polishing using diamond suspensions to obtain mirror-like surface finishes. A final chemical etching step was performed to reveal the microstructural features of interest, thereby enabling clear observation of phase distribution, porosity, and interfacial bonding under the SEM.

3. EXPERIMENTAL RESULTS AND EVALUATION

3.1. SEM Analysis Results of Samples

The microstructural characterization of the synthesized alloy specimens, which were produced via the powder metallurgy route, was meticulously carried out using scanning electron microscopy (SEM). This advanced imaging technique enabled a high-resolution visualization of the internal morphology, surface characteristics, and distribution of constituent phases within the alloyed materials. The SEM micrographs, as illustrated in Figure 1, reveal critical insights into the microstructural configuration of the samples. A detailed evaluation of the captured SEM images indicates the presence of a prominent and well-defined matrix phase, which forms the primary structural backbone of the material. This matrix appears to exhibit a high degree of continuity and cohesion, suggesting successful bonding between the compacted and sintered powder particles. Furthermore, the images display a homogeneous and isotropic dispersion of the

alloying elements and reinforcement phases throughout the matrix. This uniform distribution is indicative of effective mechanical alloying and adequate compaction during the pre-sintering stage, ultimately contributing to the microstructural integrity and performance reliability of the final alloy. The absence of significant porosity or particle agglomeration, coupled with the consistent grain morphology observed in the micrographs, further supports the quality of the processing parameters employed. These observations collectively underline the efficacy of the powder metallurgy technique in producing composite alloys with refined microstructures and well-controlled phase distributions, both of which are critical for optimizing mechanical behavior and long-term structural stability.

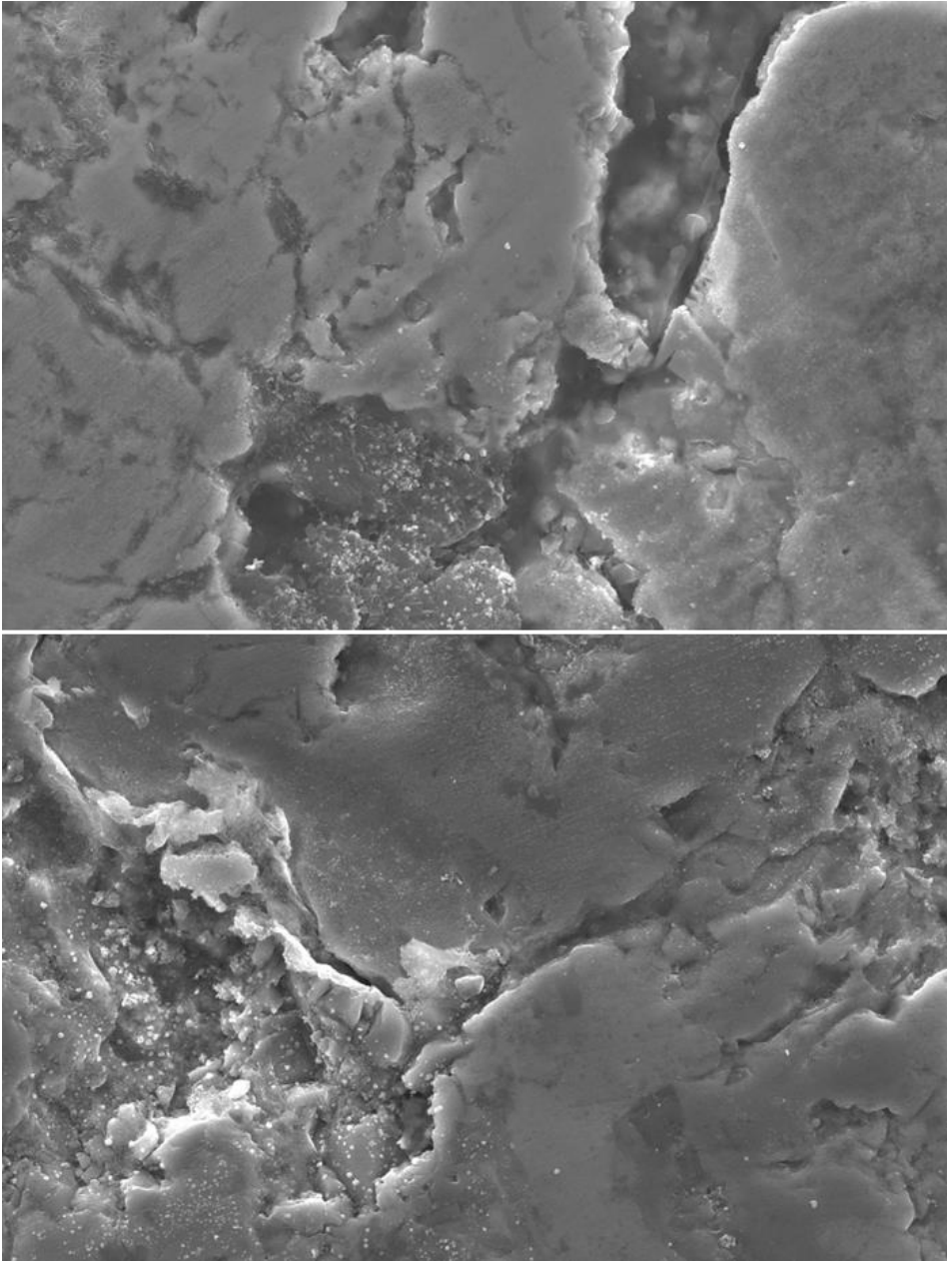


Figure 1. SEM images of the produced sample.

A comprehensive evaluation of the microstructural features of the synthesized alloy specimens was conducted using scanning electron microscopy (SEM), which provided high-resolution imagery essential for the identification and characterization of internal structural attributes. The SEM analyses revealed the occurrence of specific microstructural irregularities, most notably localized micro-cracking and the presence of porosity, both of which are widely recognized in the scientific literature as detrimental to the overall mechanical integrity of metallic systems. These structural flaws are of paramount significance due to their capacity to act as precursors to mechanical degradation, potentially leading to premature failure when the material is subjected to static or dynamic loads. The existence of microcracks is particularly concerning, as these discontinuities may serve as nucleation sites for crack propagation, functioning as stress concentrators under mechanical solicitation. Simultaneously, the formation of pores can substantially diminish the effective cross-sectional area that bears the applied load, thereby undermining the material's strength, fatigue resistance, and operational reliability [28-31]. Notably, a more refined examination of the SEM imagery—especially in specimens fabricated with optimized alloying strategies—exhibits a substantial decline in the volumetric and morphological prevalence of porosity. This reduction in porosity is highly advantageous from both a mechanical and metallurgical standpoint, as it signifies a notable enhancement in the densification behavior during the consolidation stage of the powder metallurgy process. Improved densification not only promotes superior structural cohesion and bonding among constituent particles, but also mitigates the risk of crack initiation and growth under subsequent mechanical or thermal loads. This densification is directly associated with increased interfacial integrity and load transfer efficiency, both of which are pivotal for ensuring optimal performance in engineering applications characterized by severe service conditions [32-34].

In addition to porosity mitigation, the SEM micrographs unambiguously confirm the uniform spatial distribution and fine dispersion of reinforcing phases throughout the alloy matrix. This high degree of microstructural homogeneity is indicative of the effectiveness of the fabrication methodology, which involved mechanical alloying followed by argon-atmosphere sintering at elevated temperatures. The mechanical alloying technique plays a central role in achieving thorough and intimate mixing of the elemental powders, enhancing particle-to-particle contact and promoting uniform phase distribution. Subsequently, the sintering stage facilitates atomic diffusion and metallurgical bonding between particles, which is instrumental in refining the grain structure and ensuring microstructural uniformity [35-37]. The resulting distribution of reinforcement particles is critical for achieving balanced mechanical performance, as it contributes to isotropic property enhancement, dimensional stability, and long-term durability under multiaxial stress conditions.

4. GENERAL RESULTS

Within the scope of this comprehensive experimental study, the synthesis of metallic alloy systems was successfully realized through the employment of an advanced powder metallurgy (PM) processing route. This fabrication technique was selected due to its proven capability to produce materials with controlled microstructures and superior physical and mechanical characteristics. The production methodology incorporated critical processing steps, including a cold uniaxial compaction procedure conducted under a high applied pressure of 650 MPa, which ensured the initial densification and shaping of the powder mixture. Following this compaction step, the green compacts were subjected to a sintering process performed at an elevated temperature of 1215 °C for a sustained holding time of 240 minutes. This heat treatment operation was meticulously carried out under an argon-controlled inert gas atmosphere in order to prevent undesirable oxidation reactions and to promote diffusion-driven bonding between the particles. The overall process parameters were carefully optimized with the primary objective of enhancing the final material properties, particularly in terms of structural coherence and mechanical stability.

Subsequent to the fabrication, the consolidated alloy samples were subjected to an extensive microstructural characterization using high-resolution scanning electron microscopy (SEM). This analytical technique enabled a detailed investigation of the internal features of the sintered structures, offering crucial insights into phase distribution, porosity characteristics, and interparticle bonding quality. The SEM evaluation revealed several notable outcomes, which are summarized as follows: The application of powder metallurgy as a processing methodology proved to be highly effective in the successful compaction and sintering of multi-component alloy compositions. The ability of this method to yield structurally coherent and densely packed materials underscores its technological relevance and applicability in the development of advanced engineering materials. A thorough assessment of the SEM micrographs demonstrated a systematic decrease in porosity levels with the increasing proportion of specific alloying constituents in the composite formulations. This inverse relationship between porosity and alloy content is of particular scientific and engineering significance, as a reduction in internal voids and pores generally leads to improvements in mechanical performance parameters, including tensile strength, hardness, and fracture resistance. The enhanced densification achieved via tailored alloying and sintering conditions highlights the importance of microstructural control in optimizing functional properties.

Acknowledgments

This study was conducted within the scope of the KÜBAP-01/2024-30 projects supported by Kastamonu University Scientific Research Projects Unit.

REFERENCES

1. Pradhan, P., Shadangi, Y., Shivam, V., & Mukhopadhyay, N. K. (2023). Powder metallurgical processing of CrMnFeCoMo high entropy alloy: phase evolution, microstructure, thermal stability and mechanical properties. *Journal of Alloys and Compounds*, 935, 168002.
2. Mohanty, S., Maity, T. N., Mukhopadhyay, S., Sarkar, S., Gurao, N. P., Bhowmick, S., & Biswas, K. (2017). Powder metallurgical processing of equiatomic AlCoCrFeNi high entropy alloy: Microstructure and mechanical properties. *Materials Science and Engineering: A*, 679, 299-313.
3. Torralba, J. M., Alvaredo, P., & García-Junceda, A. (2019). High-entropy alloys fabricated via powder metallurgy. A critical review. *Powder Metallurgy*, 62(2), 84-114.
4. Sharma, A., Oh, M. C., & Ahn, B. (2020). Microstructural evolution and mechanical properties of non-Cantor AlCuSiZnFe lightweight high entropy alloy processed by advanced powder metallurgy. *Materials Science and Engineering: A*, 797, 140066.
5. Akkaş, M. (2022). Synthesis and characterization of MoSi₂ particle reinforced AlCuMg composites by molten salt shielded method. *Türk Doğa ve Fen Dergisi*, 11(4), 11-17.
6. Kumar, A., Mucalo, M., Bolzoni, L., Li, Y., Kong, F., & Yang, F. (2022). Fabrication, microstructure, mechanical, and electrochemical properties of NiMnFeCu high entropy alloy from elemental powders. *Metals*, 12(1), 167.
7. Ye, W., Xie, M., Huang, Z., Wang, H., Zhou, Q., Wang, L., ... & Liu, W. (2023). Microstructure and tribological properties of in-situ carbide/CoCrFeNiMn high entropy alloy composites synthesized by flake powder metallurgy. *Tribology International*, 181, 108295.
8. Basem, A., Hassan, M. A., Elkady, O. A., El-Shekeil, Y. A., Bendoukha, S., Barhoumi, N., ... & Elsheikh, A. (2024). Characterization of FeCoNiCr high-entropy alloys manufactured by powder metallurgy technique. *Journal of Materials Research and Technology*, 30, 88-100.
9. Akkaş, M. (2024). The Effect of Molten Salt on The Mechanical Properties and Microstructure of CuNiSi Alloys with Reinforced Fe. *Science of Sintering*, 56(1).
10. Akkaş, M., K Tabonah, T. M., A Elfghi, A. M., & Özorak, C. (2023). Powder Metallurgical Fabrication Of Co Reinforced Cunisi Matrix Composites: Microstructural And Corrosion Characterization. *Technological Applied Sciences*, 18(4), 64-74.

11. Dewangan, S. K., Kumar, D., Samal, S., & Kumar, V. (2021). Microstructure and mechanical properties of nanocrystalline AlCrFeMnNiW_x (x= 0, 0.05, 0.1, 0.5) high-entropy alloys prepared by powder metallurgy route. *Journal of Materials Engineering and Performance*, 30(6), 4421-4431.
12. Moravcik, I., Cizek, J., Kovacova, Z., Nejezchlebova, J., Kitzmantel, M., Neubauer, E., ... & Dlouhy, I. (2017). Mechanical and microstructural characterization of powder metallurgy CoCrNi medium entropy alloy. *Materials Science and Engineering: A*, 701, 370-380.
13. Torralba, J. M., Alvaredo, P., & García-Junceda, A. (2020). Powder metallurgy and high-entropy alloys: update on new opportunities. *Powder Metallurgy*, 63(4), 227-236.
14. Shadangi, Y., Chattopadhyay, K., & Mukhopadhyay, N. K. (2023). Powder metallurgical processing of Al matrix composite reinforced with AlSiCrMnFeNiCu high-entropy alloys: Microstructure, thermal stability, and microhardness. *Journal of Materials Research*, 38(1), 248-264.
15. Alshataif, Y. A., Sivasankaran, S., Al-Mufadi, F. A., Alaboodi, A. S., & Ammar, H. R. (2020). Manufacturing methods, microstructural and mechanical properties evolutions of high-entropy alloys: a review. *Metals and Materials International*, 26, 1099-1133.
16. Özorak, C., Tabonah, T. M. K., & Akkaş, M. (2023). Production of CuNiSi Composites by Powder Metallurgy Method: Effects of Ti on the microstructural and corrosion properties. *European Journal of Technique (EJT)*, 13(2), 88-93.
17. Liu, G., Jiang, Y., Ma, C., Yuan, Z., Sun, B., & Shen, T. (2025). Ultrastrong nanocrystalline FeCoNiCr high entropy alloy with outstanding thermal stability. *Materials Science and Engineering: A*, 933, 148282.
18. Akkaş, M., & Elfghi, A. M. A. (2022). TiB₂ parçacık takviyeli alümin kompozitlerin üretilebilirliğinin araştırılması. *Uluslararası Doğu Anadolu Fen Mühendislik ve Tasarım Dergisi*, 4(2), 118-128.
19. Veronesi, P., Colombini, E., Rosa, R., Leonelli, C., & Garuti, M. (2017). Microwave processing of high entropy alloys: A powder metallurgy approach. *Chemical Engineering and Processing: Process Intensification*, 122, 397-403.
20. Colombini, E., Rosa, R., Trombi, L., Zadra, M., Casagrande, A., & Veronesi, P. (2018). High entropy alloys obtained by field assisted powder metallurgy route: SPS and microwave heating. *Materials Chemistry and Physics*, 210, 78-86.

21. Akkaş, M., & Al, S. F. R. A. (2021). Effect of hot pressing and reinforcement of TiC and WC on the mechanical properties and microstructure of AlCuFeCrNi HEAs alloy. *Science of Sintering*, 53(1), 19-35.
22. Verma, P. K., Singh, A., & Kumar, A. (2024). Microstructure characterization and phase evolution of equiatomic AlCoMoFeNi high entropy alloy synthesized by mechanical alloying. *Materials Chemistry and Physics*, 318, 129325.
23. Choi, H. J., & Lee, J. K. (2025). Effect of In-situ TiC Formed in the Sintering Process on the Microstructure and Mechanical Properties of NbTaVTi High Entropy Alloy. *Journal of the Japan Society of Powder and Powder Metallurgy*, 72(Supplement), S149-S152.
24. Akkaş, M., & Boushiha, K. F. I. (2021). Investigation of wc reinforced cunisi composites produced by mechanical alloying method. *El-Cezeri*, 8(2), 592-603.
25. Liu, L., Xia, H., Tang, Y., Cao, Q., Li, L., Dong, L., & Zhang, Y. (2024). Microstructure and mechanical properties of CoCrCuFeNi high-entropy alloys synthesized by powder metallurgy and spark plasma sintering. *Journal of Materials Engineering and Performance*, 33(24), 14029-14039.
26. Tian, L., Fu, M., & Xiong, W. (2018). Microstructural evolution of AlCoCrFeNiSi high-entropy alloy powder during mechanical alloying and its coating performance. *Materials*, 11(2), 320.
27. Akkaş, M. (2021). Production and characterization of boron carbide and silicon carbide reinforced copper-nickel composites by powder metallurgy method. *Materialwissenschaft und Werkstofftechnik*, 52(1), 32-42.
28. Shivam, V., Shadangi, Y., Basu, J., & Mukhopadhyay, N. K. (2020). Evolution of phases, hardness and magnetic properties of AlCoCrFeNi high entropy alloy processed by mechanical alloying. *Journal of Alloys and Compounds*, 832, 154826.
29. Moravcikova-Gouvea, L., Moravcik, I., Omasta, M., Veselý, J., Cizek, J., Minárik, P., ... & Dlouhy, I. (2020). High-strength Al0.2Co1.5CrFeNi1.5Ti high-entropy alloy produced by powder metallurgy and casting: A comparison of microstructures, mechanical and tribological properties. *Materials Characterization*, 159, 110046.
30. Salam, M. Y. A., Ogunmuyiwa, E. N., Manisa, V. K., Yahya, A., & Badruddin, I. A. (2025). Effect of fabrication techniques of high entropy alloys: a review with integration of machine learning. *Results in Engineering*, 104441.

31. Adabavazeh, Z., Hosseini, S. H., Karimzadeh, F., & Abbasi, M. H. (2025). Fabrication and performance assessment of CuFeNiMnTi high entropy alloy through mechanical alloying and spark plasma sintering. *Materials Today Communications*, 42, 111124.
32. Çetin, T., & Akkaş, M. (2020). Effect of WC reinforced on microstructure and mechanical properties of CuAlMn alloys produced by hot pressing method. *European Journal of Technique (EJT)*, 10(1), 173-183.
33. Küçükelyas, B., Çaha, İ., Kaykılarlı, C., Peters, J. C., Solak, N., Uzunsoy, D., & Gürmen, S. (2025). Synergetic effect of functionalized few-layered graphene on structural, magnetic and electrical conductivity properties of CoCuFeNi high entropy alloys. *Journal of Alloys and Compounds*, 1021, 179594.
34. Rajendrachari, S. (2022). An overview of high-entropy alloys prepared by mechanical alloying followed by the characterization of their microstructure and various properties. *Alloys*, 1(2), 116-132.
35. Abolkassem, S. A., Mohamed, L. Z., Gaber, G. A., & Elkady, O. A. (2021). Microstructure and corrosion behavior of FeNiCoCrCu and FeNiCoCrMn high entropy alloys manufactured by powder metallurgy in different acid media. *J. Mater. Res. Technol*, 10, 1122-1142.
36. Muhammad, A., Li, Y., Bing, D., Muhammad, A. R., & Muhammad, Z. S. (2025). Excelling mechanical response of a powder metallurgy medium entropy alloy under extreme loading conditions. *Powder Technology*, 120737.
37. Li, N., Wu, C., Wu, Z., Jiang, M., Hou, J., & Dong, F. (2025). Effect of Sintering Temperature and Time on Microstructure and Mechanical Properties of CoCrFeNiMn High-Entropy Alloys. *Metals*, 15(6), 591.